Master's degree in Energy Engineering
specialization in Renewable energy systems

Optimal Operation of reversible Solid Oxide Cell in Renewable Energy Communities with Hydrogen and Thermal Energy Storage

By

Di Norscia Giusy

Supervisor:
Prof. Filippo Spertino (Politecnico di Torino)
Prof. Oriol Gomis-Bellmunt (CITCEA - Universitat Politècnica de Catalunya)
Prof. Paula Muñoz Peña (CITCEA - Universitat Politècnica de Catalunya)

Politecnico di Torino
2025

Abstract

Energy communities are exploring multi-vector solutions to integrate variable renewable generation while preserving security of supply and affordability. This thesis develops an optimization-based energy management model for energy communities that enables the use of a reversible solid oxide cell (rSOC), where the rSOC can operate in electrolysis mode (SOEC) to convert electricity into hydrogen and in fuel-cell mode (SOFC) to reconvert hydrogen into electricity.

A mixed-integer linear programming (MILP) formulation is implemented in Python using Pyomo and solved with Gurobi to determine the optimal configuration over a time-resolved horizon. The multi-vector energy model optimizes electricity, heat and hydrogen flows, accounting for hydrogen storage dynamics, rSOC operating limits and mode-dependent behavior. A thermal energy storage (TES) system for cogeneration support is also included to assess the potential value of heat recovery and thermal shifting within the community's energy balance.

Simulation results show that hydrogen storage coupled with rSOC flexibility can effectively absorb surplus renewable electricity; however, this increases the total operational cost. Under the investigated assumptions, the cogeneration/TES pathway is not selected by the optimizer, indicating that its utilization is not economically or operationally justified for the studied demand and price conditions.

Table of contents

List of figures

List of tables

Chapter 1

Introduction

The increasing penetration of distributed renewable generation is changing the way local energy systems are designed and operated. In this context, energy communities are attracting growing interest as a means to improve local energy sharing, increase self-consumption and support the integration of renewable energy sources. This thesis investigates the integration of two energy communities through a storage system based on a reversible solid oxide cell.

1.1 Background

Energy communities are emerging as promising organizational frameworks for the integration of distributed renewable generation and local energy sharing. In these systems, consumers and prosumers can interact within a coordinated structure aimed at improving the use of locally generated energy and increasing the overall efficiency of the energy system [3].
Among the renewable technologies adopted in this context, photovoltaic generation plays a central role due to its widespread applicability in residential and local-scale installations [4]. However, the variability of photovoltaic (PV) generation often leads to a mismatch between local production and demand, making it necessary to develop suitable energy-sharing and flexibility strategies.
In energy communities, shared energy is often managed through virtual exchange mechanisms, while the physical electricity flows still rely on the existing distribution grid infrastructure [4]. In this framework, self-consumption, shared generation and

virtual metering become key concepts for improving the local use of renewable electricity and reducing unnecessary exchanges with the public grid [5].
Storage technologies can further support this objective by reducing both the electricity withdrawn from the grid and the surplus energy injected into it, while also increasing system flexibility [4]. For this reason, the modelling of energy communities is often formulated as an optimization problem aimed at identifying the most suitable combination of technologies, operating strategies and organizational arrangements [6].

1.2 Problem statement

Thanks to his scalability, there is a large-scale integration of PV generation in local energy systems that introduces a structural mismatch between renewable electricity production and end-use demand. Since PV output is intermittent and weather-dependent, generation does not always coincide with the temporal profile of local consumption, leading to recurring periods of excess electricity production [3].
When this surplus cannot be absorbed locally, part of the electricity is injected back into the distribution grid, potentially causing reverse power flow, i.e., a flow of electricity opposite to the conventional direction observed in passive networks. Although this work does not address these effects from an electrical protection perspective, the literature shows that such conditions may be associated with grid-related issues such as equipment stress, voltage and power quality disturbances and possible overloading of local network components [7].
In this context, the problem treated in this thesis is not only the intermittency of PV itself, but the limited capability of the local system to absorb and manage temporary surplus generation. This motivates the integration of an energy storage solution based on reversible solid oxide cell (rSOC), aimed at increasing local utilization of PV electricity, reducing reverse injection into the grid and improving the operational stability and energy autonomy of the system.
Due to the high operational temperature of the rSOC system, it is considered also a cogeneration system.

1.3 Research Objective

The main objective of this thesis is to assess the role of an rSOC-based storage system as a flexibility resource for optimizing the operation of two photovoltaic energy communities. In particular, the study investigates the economic feasibility and the potential emissions reduction associated with the integration of the storage system, with the aim of improving local energy management and increasing self-consumption.

1.4 Methodology

The methodology adopted in this thesis is based on a mixed-integer linear programming (MILP) optimization model developed in Python using Pyomo and solved with Gurobi. The model is used to optimize the operation of two photovoltaic energy communities integrating an rSOC-base storage system, accounting for the interaction between photovoltaic generation, local demand, storage operation and heat recovery from the rSOC. Because of the high operating temperature of the rSOC technology, the system is also analyzed from a cogeneration perspective, by considering the simultaneous management of electrical and thermal energy flows. The performance of the proposed configuration is then assessed through economic and environmental indicators, with particular focus on economic feasibility and CO_2 emissions reduction.

1.5 Thesis Structures

This section introduces the structure of the thesis, outlining how the discussion is organized across the various chapters.

Chapter 2 presents the methodology adopted in this work, including the system modelling approach, the optimization framework, the main assumptions considered in the analysis and the case study.

Chapter 3 reports the results obtained from the proposed model.

Chapter 4 discusses the main findings, highlighting their implications and the main limitations of the study.

Chapter 5 summarizes the main conclusions of the thesis.

Chapter 2

Methods

The second chapter provides a theoretical analysis of the proposed system, with a focus on the physical and chemical phenomena that describe the technology. The system incorporates a reversible Solid Oxide Cell (rSOC) to interconnect two distinct photovoltaic-equipped energy communities. The rSOC can operate in two modes: Solid Oxide Electrolyzer Cell (SOEC) and Solid Oxide Fuel Cell (SOFC).

2.1 System description

The proposed model aims to interconnect two energy communities, characterized primarily by residential loads, through the use of a reversible Solid Oxide Cell (rSOC) system. The rSOC is a highly flexible energy conversion device capable of operating both in power generation and fuel production modes, acting as the core hub for energy balancing. The system management follows a specific hierarchy to ensure efficiency. During periods of high solar irradiance, the photovoltaic (PV) systems first meet the immediate electric demand for communities. Any excess electricity, which would otherwise be injected into the grid causing reverse power flows, is diverted to the rSOC. In this phase, the device operates in SOEC mode to produce hydrogen, which is then stored in a dedicated tank for later use. Conversely, during the power generation phase, the rSOC functions in SOFC mode, utilizing the previously produced hydrogen to generate electricity when PV production is insufficient to meet the load. Consequently, electricity needs to be purchased from the external grid only as a last resort: when there is no hydrogen available in

the storage tank or when the stored amount is insufficient to cover the peak load. This configuration serves a dual purpose: it prevents reverse power flow into the grid - thereby avoiding operational instability - and it contributes to the system's decarbonization goals. It should be noted, however, that this dispatch priority is enforced by construction and does not account for electricity price arbitrage: in scenarios where grid electricity is temporarily cheap and no PV surplus is available, it could be economically advantageous to purchase electricity from the grid and preserve the stored hydrogen for later hours with higher electricity prices. This represents a limitation of the current formulation, which could be addressed in future work by relaxing the fixed dispatch hierarchy and allowing the optimizer to choose between grid purchase and hydrogen discharge based on real-time price signals. Additionally, the rSOC system is exploited to generate thermal energy from process waste heat during the exothermic SOFC mode. This heat is recovered in a Thermal Energy Storage (TES) to meet the facility's heating demands, substantially reducing natural gas purchased from the distribution grid and further lowering the overall CO_2 emissions. A similar rSOC-based microgrid architecture, exploiting both electrical and thermal energy to satisfy residential demands, is presented by Califano et al. [8]

The operational logic of the proposed system is shown in Figure 2.1.

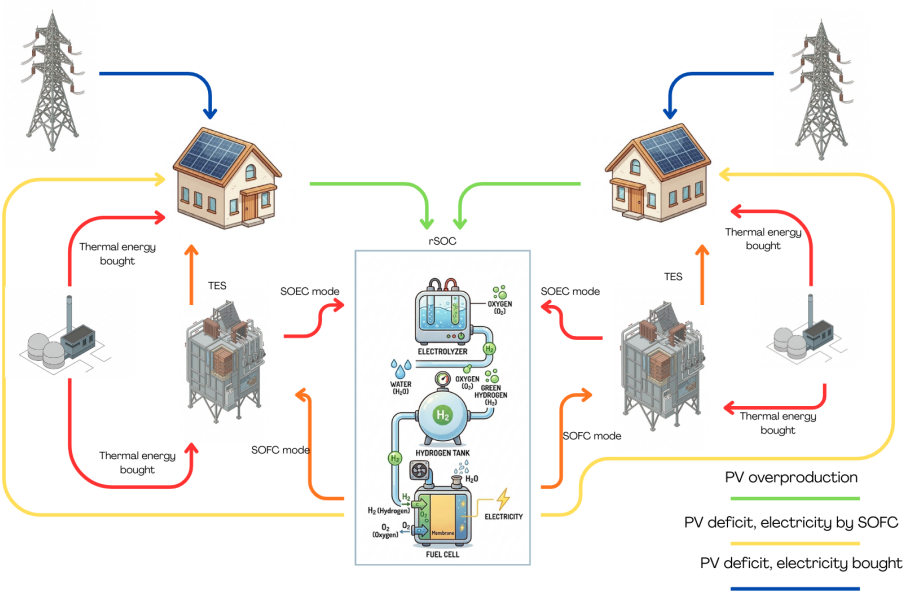

Figure 2.1: Operational Logic Diagram of the System

2.2 Mathematical formulation

This section presents the mathematical formulation of the proposed framework for representing and optimizing the overall system, including the rSOC element introduced in the previous paragraph. The formulation is structured into three parts: the physical model, the optimization model and the model flowchart.

2.2.1 Physical model

This subsection presents all the equations used to describe the system.

Photovoltaic system

Both PV systems are assumed to be existing assets and are therefore modeled as external generation profiles. For each PV system $p \in \mathscr{P}^{PV}$ and time step $t \in \mathscr{T}$, the available PV output is

$$P_{p,t}^{PV,avail} = P_p^{PV} \cdot g_{p,t}^{PV}, \tag{2.1}$$

where P_p^{PV} is the installed PV capacity and $g_{p,t}^{PV} \in [0,1]$ is the normalized PV forecast profile. This approach is consistent with the common practice of computing PV production profiles and applying them to the installed system size [6].

Reversible Solid Oxide Cell (rSOC) and hydrogen tank

At each time step $t \in \mathscr{T}$, the reversible Solid Oxide Cell (rSOC) can operate either as an electrolyzer (SOEC) consuming electricity to produce hydrogen, or as a fuel cell (SOFC) consuming hydrogen to produce electricity.
The following variables are defined:

- the electrical power absorbed in SOEC mode: $P_t^{SOEC} \geq 0$
- the electrical power generated in SOFC mode: $P_t^{SOFC} \geq 0$
- the hydrogen production: $\dot{m}_t^{H_2,prod} \geq 0$
- the hydrogen consumed: $\dot{m}_t^{H_2,cons} \geq 0$

- the hydrogen stored in the tank: H_t

The rSOC performance is parametrized using the SOEC specific electricity consumption $e^{SOFC}\ \left[\frac{kWh}{kg_{H_2}}\right]$ and the SOFC electrical efficiency η_{el}^{SOFC} (LHV-based) together with the hydrogen lower heating value $LHV_{H_2}\ \left[\frac{MJ}{kg_{H_2}}\right]$.
The electrical energy obtainable from 1 kg of hydrogen in SOFC mode is computed as:

$$e^{SOFC} = \eta_{el}^{SOFC} \cdot \frac{LHV_{H_2}}{3.6} \quad \left[\frac{kWh}{kg_{H_2}}\right] \tag{2.2}$$

where the conversion factor $1kWh = 3.6MJ$ is used [9]. Accordingly, the electricity-hydrogen conversion in SOEC mode is modelled as

$$\dot{m}_t^{H_2,prod} = \frac{P_t^{SOEC}}{e^{SOFC}} \tag{2.3}$$

and SOFC mode as

$$P_t^{SOFC} = e^{SOFC} \cdot \dot{m}_t^{H_2,cons}\ . \tag{2.4}$$

Hydrogen storage is represented through a mass balance and a capacity constraint:

$$H_t = H_{t-1} + \dot{m}_t^{H_2,prod} \cdot \Delta t - \dot{m}_t^{H_2,cons}\ , \tag{2.5}$$

$$0 \leq H_t \leq H^{max}\ , \tag{2.6}$$

where Δt is the time-step duration (equal to 1 h) and H^{max} is the tank capacity.

Thermal Energy Storage (TES)

In addition to electrical power, a reversible solid oxide cell (rSOC) exchanges thermal power with the rest of the plant. In SOFC mode, the stack releases heat that can be recovered and stored, whereas in SOEC mode the stack may require an external heat supply, which can be provided by a thermal energy storage (TES) [10].
Latent heat thermal energy storage (LHTES) exploits the latent heat associated with a phase transition of the storage medium during the charging (heat absorption) and discharging (heat release) process:

$$Q = \dot{m}[C_{ps}(T_m - T_s) + h + C_{pl}(T_l - T_m)] \tag{2.7}$$

where Q is the stored heat, $\dot{m}$ is the mass flow rate, C_{ps} is the specific heat capacity of the solid phase, T_m is the melting temperature, T_s is the initial solid-phase temperature, h is the latent heat of fusion, C_{pl} is the specific heat capacity of the liquid phase and T_l is the final liquid-phase temperature.
In an LHTES system, the phase-change material (PCM) absorbs or release a large amount of heat at an almost constant temperature during melting/solidification, enabling quasi-isothermal heat exchange and relatively high storage energy density compared with sensible-heat storage. For practical TES applications, the phase transition of interest is most often the solid-liquid one, because it provides large enthalpy changes while avoiding the large volume/density variations and containment challenges typically associated with liquid-gas transitions. Accordingly, it is possible to realize TES with medium-to-high specific energy at an approximately constant temperature, which is one of the main advantages of PCM-based storage [1].

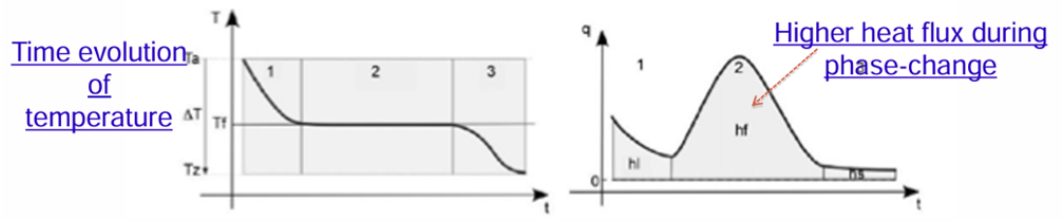

Figure 2.2: Qualitative profiles of temperature and heat flux for a PCM undergoing melting (latent-heat storage region). Reproduced from [1]

To obtain a compact model suitable for system-level simulations, the rSOC thermal exchange is expressed as proportional to the hydrogen mass flow rate through mode-dependent specific coefficients k^{SOEC} and k^{SOFC}, with units $\left[\frac{kWh}{kg}\right]$. These coefficients are derived from the reaction enthalpy (that is evaluated in the following chapter) Δh expressed on a molar basis, by converting mol to kg through the hydrogen molar mass MW_{H_2}, and converting kJ to kWh through the factor $\frac{1}{3600}$:

$$k = \frac{\Delta h}{MW_{H_2}} \cdot \frac{1}{3600} \quad \left[\frac{kWh}{kg}\right] \tag{2.8}$$

As introduced above, $\dot{m}_t^{H_2,prod}$ being the hydrogen production mass flow rate in SOEC mode and $\dot{m}_t^{H_2,cons}$ being the hydrogen consumption mass flow rate, the

associated thermal power terms are defined as:

$$Q_t^{SOEC} = \dot{m}_t^{H_2,prod} \cdot k^{SOEC} \ , \tag{2.9}$$

$$Q_t^{SOFC} = \dot{m}_t^{H_2,cons} \cdot k^{SOFC} \ . \tag{2.10}$$

With this formulation, Q_t^{SOEC} represents the thermal power linked to electrolysis operation, that represent the heat demand of the rSOC and needs to be covered by the TES or the heaters; while Q_t^{SOFC} represents the thermal power made available during fuel-cell operation, potentially recoverable and storable in TES [8].
The TES is modelled through a round-trip efficiency RTE_{TES}, which accounts for thermal losses during charging and discharging; accordingly, the thermal energy effectively accumulated in the TES and the energy effectively delivered from the TES are computed as functions of the TES power flow and RTE_{TES}. In particular, following the adopted convention, RTE_{TES} can be expressed as the product of a charging efficiency $\eta_{in,TES}$ and a discharging efficiency $\eta_{out,TES}$ [10]:

$$RTE_{TES} = \eta_{in,TES} \cdot \eta_{out,TES} \tag{2.11}$$

In this work, the charging and discharging efficiencies are assumed to be equal and symmetrical, such that:

$$\eta_{in,TES} = \eta_{out,TES} = \sqrt{RTE_{TES}} \tag{2.12}$$

Accordingly, the energy effectively accumulated in the TES during a charging phase ($Q_{in,j}$) and the energy effectively delivered during a discharging phase ($Q_{out,j}$) are written as a function of the thermal power $P_{th,TES,j}$ exchanged over the time step t_j [8]:

$$Q_{in,j} = \sqrt{RTE_{TES}} \cdot P_{th,TES,j} \cdot t_j \ , \tag{2.13}$$

$$Q_{out,j} = \frac{P_{th,TES,j} \cdot t_j}{\sqrt{RTE_{TES}}} \ . \tag{2.14}$$

In this notation, $P_{th,TES,j}$ represents the thermal power flow at the TES boundary; $Q_{in,j}$ is the fraction of energy that actually enters the storage after charging losses, while $Q_{out,j}$ is the energy internal to the storage that must be depleted to provide the required power $P_{th,TES,j}$ to the system.

Constraint

This section defines the overall constraints used to couple the electrical balance with the hydrogen subsystem and the thermal balance, including the logical "switches" that distinguish deficit from overproduction regimes.
Time is discretized over $t \in \mathscr{T}$.
The key external inputs are the available PV electricity output $P_{p,t}^{PV,avail}$, the electric demand D_t and the thermal demand Q_t^{dem}.
Main decision variables include:

- surplus indicator $s_t \in \{0,1\}$;
- operating mode indicators $u_t^{EC}, u_t^{FC} \in \{0,1\}$;
- switching indicator $w_t \in \{0,1\}$;
- overproduction $OP_t \geq 0$;
- deficit $DEF_t \geq 0$;
- hydrogen production/consumption $\dot{m}_t^{H_2,prod}, \dot{m}_t^{H_2,cons} \geq 0$;
- fuel-cell electricity $E_t^{FC} \geq 0$;
- grid purchase $E_t^{grid} \geq 0$;
- tank inventory H_t ;
- TES variables $(E_t^{TES}, Q_{in,j}, Q_{out,j})$.

A binary variable s_t activates either overproduction ($P_{p,t}^{PV,avail} \geq D_t$) using Big-M constraints (with M an upper bound, e.g., $M \geq max_t \left\{ \left| P_{p,t}^{PV,avail} - D_t \right| \right\}$).
The logic is enforced as:

$$P_{p,t}^{PV,avail} - D_t \leq M \cdot s_t \ , \tag{2.15}$$

$$D_t - P_{p,t}^{PV,avail} \leq M \cdot (1 - s_t) \ . \tag{2.16}$$

This construction makes $s_t = 1$ consistent with the surplus and $s_t = 0$ consistent with deficit.

Overproduction is defined as the non-negative part of the PV-demand difference and forced to zero in deficit mode (with the Big-M, this time indicated as M_{OP}):

$$OP_t \geq P_{p,t}^{PV,avail} - D_t \ , \tag{2.17}$$

$$OP_t \leq M_{OP} \cdot s_t \ . \tag{2.18}$$

Similarly, the deficit variable represents the non-negative part of $D_t - P_{p,t}^{PV,avail}$ and is forced to zero in surplus mode (with the Big-M):

$$DEF_t \leq D_t - P_{p,t}^{PV,avail} + M \cdot s_t \ , \tag{2.19}$$

$$DEF_t \geq D_t - P_{p,t}^{PV,avail} - M \cdot s_t \ , \tag{2.20}$$

$$DEF_t \leq M \cdot (1 - s_t) \ . \tag{2.21}$$

The SOEC is linked to surplus and the SOFC to deficit through mode indicators:

$$u_t^{EC} = s_t \ , \tag{2.22}$$

$$u_t^{FC} = 1 - s_t \ . \tag{2.23}$$

Switching is tracked by w_t as the change in SOEC commitment between consecutive time steps (for $t > t_0$):

$$w_t \geq u_t^{EC} - u_{t-1}^{EC} \ , \tag{2.24}$$

$$w_t \geq u_{t-1}^{EC} - u_t^{EC} \ . \tag{2.25}$$

Together, these two constraints enforce $w_t \geq |u_t^{EC} - u_{t-1}^{EC}|$, capturing mode transitions in both directions -from SOEC to SOFC and from SOFC to SOEC. This is the standard linearization of the absolute value for binary variable. To penalize operation during switching, an auxiliary variable A_t is introduced to represent a "reduced usable overproduction", approximating $A_t \approx OP_t(1 - 0.5 \cdot w_t)$ via linear inequalities:

$$A_t \leq OP_t \ , \tag{2.26}$$

$$A_t \geq OP_t - 0.5 \cdot M_A \cdot w_t \ . \tag{2.27}$$

In this way, it is possible to avoid overestimating hydrogen production or consumption during an rSOC operation switch. This approach accounts for half of the

theoretical amount, assuming a switching time of 30 minutes [8].
Hydrogen production is driven by penalized surplus electricity using the SOEC specific consumption e^{SOEC}:

$$\dot{m}_t^{H_2,prod} \leq \frac{A_t}{e^{SOEC}} \ . \tag{2.28}$$

In deficit hours, hydrogen can be consumed by the SOFC to generate electricity with yield e^{SOFC}:

$$\dot{m}_t^{H_2,cons} \leq \frac{DEF_t}{e^{SOFC}} \ , \tag{2.29}$$

$$E_t^{FC} = \dot{m}_t^{H_2,cons} \cdot e^{SOFC} \ , \tag{2.30}$$

$$DEF_t = E_t^{FC} + E_t^{grid} \ , \tag{2.31}$$

deficit is covered by SOFC generation and grid purchase. Additional Big-M bounds are used to force the hydrogen consumption only when $u_t^{FC} = 1$ occurs. The hydrogen inventory is bounded by tank capacity and updated through in/out flows (with initial condition at t_0:

$$0 \leq H_t \leq H^{max} \ , \tag{2.32}$$

$$H_t = H_{t-1} + H_t^{to} - H_t^{from} \quad (for\ t > t_0) \ , \tag{2.33}$$

with H_{t_0} set by the initial stock.
Production/consumption are linked to tank flows (all produced H_2 goes to the tank, and all consumed H_2 is withdrawn):

$$\dot{m}_t^{H_2,prod} = H_t^0 \ , \tag{2.34}$$

$$\dot{m}_t^{H_2,cons} = H_t^{from} \ . \tag{2.35}$$

On the thermal side, a plant-level rSOC net thermal power is introduced as:

$$P_t^{rSOC,th} = Q_t^{SOFC} - Q_t^{SOEC} \ , \tag{2.36}$$

with a sign convention where $P_t^{rSOC,th} > 0$ means net heat delivered to the system and $P_t^{rSOC,th} < 0$ net heat absorbed (e.g., during SOEC operation).
Finally, the overall thermal balance couples rSOC heat, TES charge/discharge, boiler

output and the thermal demand:

$$P_t^{boil} + P_t^{rSOC,th} + Q_t^{out} - Q_t^{in} = Q_t^{dem} \ . \tag{2.37}$$

The complete Python implementation of the hydrogen system model - which represents the core computational contribution of this work - is reported in Appendix A.

2.2.2 Optimization model

General formulation

This section presents the general optimization problem used to compute the optimal operation of the system over a discrete time horizon. The model is formulated as a linear program based on nodal energy balances and technical operating limits. Time is discretized into a finite set of time steps $t \in \mathscr{T}$. Given the constraints defined above, the optimization minimizes the total system cost and the associated CO_2 emissions, either through a weighted-sum objective or by treating one metric as constraint.

A constant real discount rate r is used to compute the present value of replacement expenditures occuring during the project lifetime L $(years)$.
For each component k, a replacement may occur every y_k years, with a replacement cost per event C_k^{repl}. The integer number of replacements within the project lifetime L is:

$$N_k = \frac{L}{y_k} \tag{2.38}$$

and the discounted total replacement cost is:

$$C_k^{repl} = \sum_{i=1}^{N_k} \frac{C_k^{repl}}{(1+r)^{iy_k}} \tag{2.39}$$

where iy_k denotes the number of years from the base year ($t = 0$) to the i-th replacement event (i.e., replacements occur at years $y_k, 2y_k, ..., N_k y_k$). C_k^{repl} is a standard present-value discounting of cash flows. In the implementation, this discounted replacement term is computed for PV, rSOC, the H_2 tank, TES and cables.

Component investment costs are computed from a sizing variable (or rated power) multiplied by a specific CAPEX. For instance, for the SOEC unit (rated electrical power P_{SOEC} in kW):

$$C_{SOEC}^{capex} = c_{SOEC}^{capex} \cdot P_{SOEC} \tag{2.40}$$

and similarly the fixed annual OPEX is:

$$C_{SOEC}^{opex} = c_{SOEC}^{opex} \cdot P_{SOEC} \ . \tag{2.41}$$

This cost structure (size times specific cost) is commonly used in linear energy models [11].
The decision to size the rSOC based on the electrical power required in SOEC mode (rather than on the power produced in SOFC mode) is motivated by the fact that, under comparable operating conditions, the SOEC electrical demand is higher than the SOFC electrical output. Moreover, the cell is subject to a physical limit on current density (A/cm^2); operation in SOEC mode typically brings the cell closer to this limit. Therefore, sizing the stack based on SOFC operation would underestimate the required active area and could result in an undersized design when the system operates in SOEC mode [12].

For storage capacities that are decision variables, the model uses "max-over-time" constraints to define the required installed capacity. For the H_2 tank [13]:

$$H^{max} \geq H_t \quad \forall t \in \mathscr{T} \tag{2.42}$$

where H_t is the stored hydrogen inventory, and H^{max} is the tank size decision variable. The tank CAPEX and OPEX then become:

$$C_{\text{tank}}^{\text{capex}} = c_{\text{tank}}^{\text{capex}} \cdot H^{\text{max}} \tag{2.43}$$
$$C_{\text{tank}}^{\text{opex}} = c_{\text{tank}}^{\text{opex}} \cdot H^{\text{max}} \tag{2.44}$$

An analogous set of equations is used for TES capacity E_{TES}^{max} based on the stored thermal energy trajectory:

$$C_{\text{TES}}^{\text{capex}} = c_{\text{TES}}^{\text{capex}} \cdot E_{TES}^{\text{max}} \tag{2.45}$$
$$C_{\text{TES}}^{\text{opex}} = c_{\text{TES}}^{\text{opex}} \cdot E_{TES}^{\text{max}} \tag{2.46}$$

The costs related to the new cables needed are also taken into account. The cable CAPEX is computed from the physical quantity of cable installed. For a given line i and cable type j, the installed mass is $l_i w_j$ $[kg]$, and the corresponding cost is $l_i w_j c_j^{kg}$ $[€]$. Using the binary selection variables, the total cable CAPEX is expressed as

$$C_{cables}^{capex} = \sum_{i \in \mathscr{L}} \sum_{j \in \mathscr{C}} x_{i,j} l_i w_j c_j^{kg} \,, \tag{2.47}$$

where $x_{i,j} \in \{0,1\}$ is a binary variable selecting cable type j for line i, l_i $[km]$ is the length of line i, w_j $[\frac{kg}{km}]$ is the linear weight of cable type j and c_j^{kg} $[\frac{€}{kg}]$ is the corresponding unit purchase cost. A detailed description of the cable catalogue, the binary selection logic and the sizing constraints is provided in Section 2.3.4. Operating and maintenance expenditures for cables are modelled with a simplified proportional approach, assuming that annual OPEX is a fixed fraction α of the investment cost:

$$C_{cables}^{opex} = \alpha \cdot C_{cables}^{capex} \,. \tag{2.48}$$

Total plant CAPEX and fixed OPEX are obtained by summing across components:

$$C_{\text{tot}}^{\text{capex}} = \sum_{k \in \mathscr{K}_{\text{capex}}} C_k^{\text{capex}}, \tag{2.49}$$

$$C_{\text{tot}}^{\text{opex}} = \sum_{k \in \mathscr{K}_{\text{opex}}} C_k^{\text{opex}}. \tag{2.50}$$

where the set $\mathscr{K}_{\text{capex}}$ includes rSOC, H_2 tank, TES and cables; and $\mathscr{K}_{\text{opex}}$ includes the same components as $\mathscr{K}_{\text{capex}}$ plus PV. The PV system is assumed to be a pre-existing asset, therefore its CAPEX cost is not considered in $\mathscr{K}_{\text{capex}}$.
Finally, the total present-value investment cost is upfront CAPEX plus discounted replacements over the lifetime:

$$C_{\text{inv}} = C_{\text{tot}}^{\text{capex}} + \sum_{k \in \mathscr{K}_{\text{repl}}} C_k^{\text{repl}} \tag{2.51}$$

where the set $\mathscr{K}_{\text{repl}}$ is equivalent to $\mathscr{K}_{\text{opex}}$. The annual operating cost is computed as the sum of fixed OPEX and variable energy expenditures. With electricity bought

from the grid E_t^{buy} and an electricity price π_t^{el} $\left(\frac{€}{MWh}\right)$, the electricity expenditure is:

$$C^{el} = \sum_{t \in \mathscr{T}} E_t^{buy} \frac{\pi_t^{el}}{1000} \tag{2.52}$$

where division by 1000 converts $\frac{€}{MWh}$ into $\frac{€}{kWh}$, since E_t^{buy} is in kWh. Similarly, the thermal demand is met by gas boilers represented through a gas-energy input E_t^{gas}, implemented as $P_{boiler,t}$ in kWh per time step, with gas price π_t^{gas}:

$$C^{gas} = \sum_{t \in \mathscr{T}} E_t^{gas} \frac{\pi_t^{gas}}{1000} \ . \tag{2.53}$$

Therefore, the total annual cost is:

$$C_{ann} = C_{tot}^{opex} + C^{el} + C^{gas} \tag{2.54}$$

which matches the common "fixed + variable" operating cost structure in LP energy models [14]. It is also necessary to define a total discounted cost, that is evaluated as follows:

$$C_{tot}^{disc} = \sum_{i=1}^{L} \frac{C_{ann}}{(1+r)^i} \tag{2.55}$$

where L is the lifetime of the project, C_{ann} is the total annual cost and r is the discount rate.

A baseline reference annual cost is computed to quantify economic savings with respect to the pre-retrofit configuration. The baseline accounts for the electricity deficit, so the energy that would have been purchased without the new system, and the full thermal demand supplied by gas:

$$C_{ann}^{ref} = \sum_{t \in \mathscr{T}} E_t^{def} \frac{\pi_t^{el}}{1000} + \sum_{t \in \mathscr{T}} Q_t^{th} \frac{\pi_t^{gas}}{1000} \ . \tag{2.56}$$

Regarding the carbon footprint, γ^{el} is the grid emission factor $\left[\frac{kgCO_2}{kWh}\right]$ and γ^{gas} is the gas emission factor $\left[\frac{kgCO_2}{kWh}\right]$. The baseline emissions are:

$$CO2_{el}^{ref} = \sum_{t \in \mathscr{T}} \gamma^{el} E_t^{def} \ , \tag{2.57}$$

$$CO2_{gas}^{ref} = \sum_{t \in \mathscr{T}} \gamma^{gas} Q_t^{th} \,, \tag{2.58}$$

$$CO2_{tot}^{ref} = CO2_{el}^{ref} + CO2_{gas}^{ref} \,. \tag{2.59}$$

The system emissions are computed analogously, replacing E_t^{def} with the actual grid purchases E_t^{buy}, and using the boiler gas input for the thermal part:

$$CO2_{el}^{sys} = \sum_{t \in \mathscr{T}} \gamma^{el} E_t^{buy} \,, \tag{2.60}$$

$$CO2_{gas}^{sys} = \sum_{t \in \mathscr{T}} \gamma^{gas} E_t^{gas} \,, \tag{2.61}$$

$$CO2_{tot}^{sys} = CO2_{el}^{sys} + CO2_{gas}^{sys} \,. \tag{2.62}$$

This approach is standard in energy system accounting and optimization [15]. The absolute emissions reduction is defined as:

$$\Delta CO2 = CO2_{tot}^{ref} - CO2_{tot}^{sys} \tag{2.63}$$

so that $\Delta CO2 > 0$ indicates an emissions reduction. The percentage reduction is:

$$\Delta CO2\% = \frac{\Delta CO2}{CO2_{tot}^{ref}} \cdot 100 \tag{2.64}$$

which provides a normalized measure of improvement relative to the baseline.

To address the trade-off between economic performance and environmental impact, the operation problem is formulated as bi-objective optimization and solved by combining both objectives into a single aggregate function.
Specifically, the two criteria considered are the total system cost C_{tot}^{sys} and the absolute CO_2 reduction with respect to the baseline, $\Delta CO2$, where the C_{tot}^{sys} is evaluated as:

$$C_{tot}^{sys} = C^{inv} + C_{tot}^{disc} \,. \tag{2.65}$$

In the weighted-sum formulation, the cost and emissions objectives have different units and typical magnitudes. To avoid that the numerically larger objective dominates the scalarized problem, both criteria are normalized before being combined into the aggregate objective function. Following standard recommendations in multi-objective optimization, each objective is scaled by a characteristic range so that the

resulting normalized quantities are of a comparable order of magnitude [16]. In this work approximate range-based scaling factors are adopted, based on the expected order of the metrics in the case study (100 k€ for cost and 10 $t\mathrm{CO}_2/year$ for CO_2 reduction). This leads to dimensionless normalized objectives of order one, so that the weights w_{cost} and w_{carbon} can be interpreted as genuine preference parameters. The resulting objective function is written as:

$$minJ = w_{cost} \cdot \hat{C}_{tot}^{sys} - w_{carbon} \cdot \Delta\hat{\mathrm{CO}}_2 \ , \tag{2.66}$$

where $w_{cost} \in [0,1]$ expresses the relative preference assigned to cost minimization and $w_{carbon} \in [0,1]$ expresses one assigned to $\Delta\mathrm{CO}_2$ reduction. The relation between the two weights is $w_{cost} + w_{carbon} = 1$.

Linear and mixed-integer linear programming formulation

The operational planning and sizing problem described in this chapter is formulated as a mixed-integer linear problem (MILP). All constraints are expressed as linear equalities or inequalities in the decision variables, and the objective function is linear in costs and emissions. The model includes both continuous variables and binary variables, which leads to a MILP structure rather than a purely continuous linear program (LP) [17].

Binary variables are used to capture discrete operating regimes and logical decisions that cannot be represented in a purely continuous framework without introducing non-linearities. In particular, the surplus indicator s_t and the mode indicators u_t^{EC} and u_t^{FC} distinguish between surplus and deficit conditions and enforce mutually exclusive SOEC/SOFC operation. The switching variable w_t tracks changes in rSOC operating mode between consecutive time steps, enabling a penalization of production/consumption during transitions. In the electrical connection model, the binary variable $x_{i,j}$ implement the selection of a single cable type j for each line i, linking the discrete cable catalogue to the continuous current and cost calculations.

Logical relations and piecewise definitions (e.g., surplus vs. deficit, charging vs. discharging, cable oversizing limits) are reformulated through standard Big-M constraints, so that all resulting expressions remain linear in the decision variables. In each, the Big-M parameter is chosen as a valid upper bound for the corresponding physical quantity, in order to avoid numerical issues while preserving correctness of the logical conditions. With this construction, non-linear mode-switching behaviour

of the rSOC and the TES is approximated by a set of linear constraints involving binary variables, which is a common strategy in energy-system MILP models.
The overall problem remains a single large-scale MILP defined over the horizon $\mathscr{T}$, where the time-coupling arises mainly from storage dynamics and from the definition of investment capacities as maximum over time. Once all physical, economic and emission-related constraints are assembled, the resulting MILP problem is solved by minimizing the aggregate objective function. This model is implemented in Python using the Pyomo algebraic modelling language [18], and it is solved with the commercial MILP solver Gurobi [19], which ensures global optimality by reaching the predefined optimal gap.
Specific solver settings are adopted to effectively balance solution accuracy with computation effort. In particular, the optimality gap is tuned to ensure high-quality results while maintaining manageable runtimes. A relative MIP optimality gap of 2% and a maximum time of 1200 s per run are used. These stopping criteria ensure that the search terminates once a feasible solution within 2% of the best known bound is found or when the time limit is reached, whichever is reached first. In addition, several parameters are tuned to accelerate the search for good incumbent solutions:

- $MIPFocus = 1$ directs the solver to prioritize finding feasible solutions;
- $Heuristics = 0.15$ allocates 15% of the time budget to primal heuristics;
- $Cuts = 2$ and $Presolve = 2$ enable aggressive cutting planes and presolve reductions, respectively, reducing the effective problem size;
- $Threads = 4$ to match the available hardware resources and ensure reproducible computational performance.

2.2.3 Model flowchart

Figure 2.3 provides the flowchart of the proposed optimization model, summarizing the workflow from data collection to sizing optimization and results assessment.

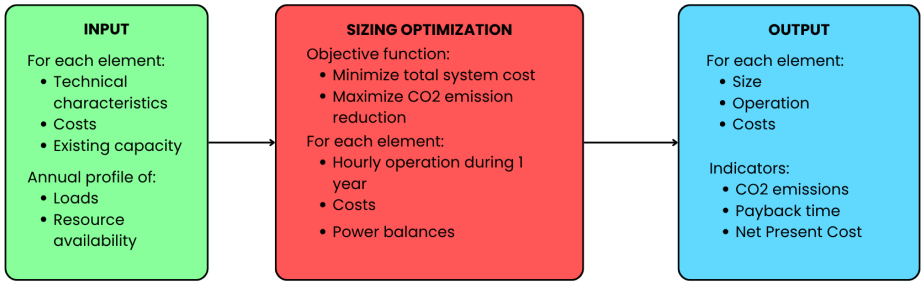

Figure 2.3: Flowchart of the methodology

As shown in the figure, the input stage collects the techno-economic characteristics of each component (including costs and existing capacity) together with annual profiles of loads and resource availability. These data feed the sizing-and-operation optimization, which determines an hourly operating strategy over one representative year while enforcing power-balance constraints and evaluating costs and emissions according to the selected objective functions. The model then delivers the optimal system configuration and operation, and computes the main performance indicators, including CO_2 emissions, payback time and net present cost.

2.3 Case study and data

This chapter presents the case study application of the system described in the previous chapters, which is assumed to be located in Catalonia (Spain). The objective is to assess the system performance under realistic territorial conditions, while keeping the modelling framework unchanged. In particular, the geographical separation between the two energy communities is set equal to the real-world distance between two existing communities, located in Santa Maria de Palautordera (Barcelona) [20]. In particular, both the communities are part of La Lleva Comunitat Energètica [21].

The approximate distance between the two energy communities is about 800 m (straight-line distance), estimated using the distance measurement tool in Google Earth [22]. However, since detailed operational data for these communities are not publicly available, the corresponding demand and usage profiles are reconstructed through estimates based on the assumptions described in this sections. This choice enables a spatially realistic setup while ensuring consistency with the available input data and the adopted modelling approach.

Due to the complexity of the system, a number of assumptions are introduced to simplify the problem formulation. First, the energy communities and their installed photovoltaic capacity are assumed to be already in place; therefore, installation costs are excluded, and only operation and maintenance costs, as well as replacement costs are considered. Furthermore, converters and auxiliary systems are not included in the simulation.

2.3.1 Electricity and heat demand profiles and scaling factors

Hourly electricity-demand data for Catalonia were downloaded from the Catalonia transparency open-data portal [23]. The data refer to year 2024, which is the most recent year available from the selected source at the time of access. For the energy communities case study, the contracted electric power is set to 4.6 kW per residence, since this is the most commonly contracted value in Spain [24]. The maximum power in Catalunia is taken as $P_{max,Catalunya} = 7047.77\ MW$ [23]. A simultaneity factor is also considered; since each energy community is modeled as a single dwelling, C_s results to 1 [25]. Using these values, it is possible to evaluate the scaling factor as

$$k_s = \frac{C_s \cdot P_{\text{contr}}}{P_{\text{max,Catalonia}}} \tag{2.67}$$

where k_s is the scaling factor, C_s is the simultaneity factor, P_{contr} is the contracted power and $P_{\text{max,Catalonia}}$ is the maximum power in Catalonia expressed in kW. The resulting value is $k_s = 6,52689E-07$, and it is applied to both the energy communities cases.

Regarding thermal demand, data from 2022 Energy Balance of Catalonia published by the Institut Català d'Energia (ICAEN) are used, as 2022 was the most

recent year available from the selected source at the time of access [26]. The dataset reports energy use by sector and by energy carrier. Focusing on the domestic sector and summing the contribution of all relevant carriers, the total domestic thermal demand for Catalonia is estimated. The carriers considered are "Petroleum and petroleum products", "Natural gas" and "Renewable energies", the latter including "Solar thermal energy", "Agricultural, animal and forestry biomass", "Biogas", "Ambient heat (heat pumps)". The resulting total domestic demand is 1251.364568 kTEP, that is converted to 14553369927 kWh using the coversion factors in [27].

To derive an hourly heat-demand profile over the year, the Heating Degree Days (HDD) approach is adopted as a temperature-based proxy for space-heating needs [28]. The method requires outdoor air temperature data; however, the selected dataset provides only monthly mean temperatures. Therefore, the monthly mean temperature is assumed to be representative of all days within the same month [29]. Under this assumption, the monthly HDD for each month m is computed as

$$HHD_{monthly,m} = n_m \cdot max(T_{base} - T_{av,m}, 0) \tag{2.68}$$

where n_m is the number of days in the month m, $T_{base} = 15°C$ is the reference temperature [30], the $T_{av,m}$ is the monthly mean outdoor temperature for the month m from the Meteocat [29]. The $max(T_{base} - T_{av,m}, 0)$ ensures that only positive values can result. The corresponding daily HDD is then obtained as

$$HHD_{day,m} = \frac{HHD_{monthly,m}}{n_m}. \tag{2.69}$$

Table 2.1 summarize the inputs (n_m, $T_{av,m}$) and the computed indicators ($HHD_{monthly,m}$, $HHD_{day,m}$).

Table 2.1: Monthly heating degree days (HDD)

Month	n_m [d]	$T_{av,m}$ [°C]	T_{base} [°C]	$HDD_{monthly,m}$ [°C·d]	$HDD_{day,m}$ [°C·d/d]
January	31	10.2	15	148.8	4.8
February	28	11.8	15	89.6	3.2
March	31	10.8	15	130.2	4.2
April	30	14.1	15	27.0	0.9
May	31	20.7	15	0.0	0.0
June	30	24.7	15	0.0	0.0
July	31	26.7	15	0.0	0.0
August	31	27.2	15	0.0	0.0
September	30	22.5	15	0.0	0.0
October	31	20.7	15	0.0	0.0
November	30	15.2	15	0.0	0.0
December	31	12.6	15	74.4	2.4
Total				470.0	

For the purposes of estimating the daily thermal energy demand over a full year, the annual demand profile is decomposed into a climate-dependent component, indicated as E_{clime}, associated with the space-heating service, and a use-dependent component, indicated as E_{DHW}, associated with domestic hot water production. This disaggregation is consistent with the Spanish regulatory framework set by the Código Técnico de la Edificación (Real Decreto 314/2006) and its Documento Básico de Ahorro de Energía [31], which requires that energy calculations allow the breakdown of final energy use by building technical services, explicitly including heating and DHW as separate items. For the $E_{DHW,d}$ component, in the absence of detailed end-use data for building stock under analysis, an approximation based on national statistics is adopted: an IDAE practical guide reports a typical household end-use split in which DHW is on the order of 20-25% (indicative values reported: 21% for DHW and 46% for space heating) [32]. Consistent with this order of magnitude, the present model assumes $E_{DHW,d} = 0.25 \cdot E_{tot,d}$ and therefore $E_{clime,d} = E_{tot,d} - E_{DHW,d}$. It is important to underline that the 25% value is a modelling assumption derived from statistical evidence (IDAE) rather than a parameter prescribed by DB-HE. DB-HE regulates DHW demand through reference procedures/values while the percentage is used here for an aggregate, top-down estimate.

Table 2.2: Assumed split of total daily thermal energy demand into climate-dependent (space heating) and use-dependent (DHW) components.

Component	Symbol	Share of $E_{tot,d}$
Domestic hot water (use-dependent)	$E_{DHW,d}$	0.25
Space heating (climate-dependent)	$E_{clime,d}$	0.75

Concerning the evaluation of the hourly thermal energy demand over an entire year, the methodology follows the same logic adopted for the daily profile, starting from the reconstruction of the hourly outdoor air temperature. To this end, the hourly temperature is approximated through a harmonic (sinusoidal) model, in which the temperature evolution is described by a mean value, an amplitude, and a phase shift (i.e., the timing of the peak)

$$T(t) \approx T_{avg} + A \cdot cos\left(\frac{2\pi}{24}(t - t_{peak})\right) \tag{2.70}$$

where T_{avg} denotes the average air temperature and A is the diurnal amplitude, computed as $A = \frac{T_{max} - T_{min}}{2}$, with the T_{max} and T_{min} being the daily maximum and minimum temperatures, respectively. Here, t represents the hour of the day (local time), and t_{peak} is the time of the daily temperature maximum; in this work, t_{peak} is assumed to occur at 14:00. This formulation is consistent with harmonic regression approaches commonly used to represent periodic (seasonal) patterns through sine and cosine terms [33]. The input data required to define the method-namely average, maximum and minimum temperatures-are retrieved from the MeteoCat database [34]:

Table 2.3: Monthly outdoor air temperatures used as inputs for the harmonic (sinusoidal) hourly temperature model

Month	$T_{avg,m}$ [°C]	$T_{min,m}$ [°C]	$T_{max,m}$ [°C]	A_m [°C]
January	10.2	6.3	14.1	3.90
February	11.8	7.5	16.2	4.35
March	10.8	8.3	14.2	2.95
April	14.1	9.9	18.3	4.20
May	20.7	15.8	25.6	4.90
June	24.7	19.5	30.0	5.25
July	26.7	21.9	31.6	4.85
August	27.2	21.8	32.6	5.40
September	22.5	18.1	26.9	4.40
October	20.7	17.0	24.4	3.70
November	15.2	11.2	19.2	4.00
December	12.6	9.4	15.9	3.25

Since only monthly data are available, the corresponding value is assumed to be constant throughout the month and is therefore applied to each day within that month.

Building on the daily demand formulation, the same approach is extended to an hourly resolution. Accordingly, the hourly thermal demand is expressed as the sum of an hourly climate component and an hourly DHW-use component.

$$E_{tot,h} = E_{clime,h} + E_{DHW,h} \tag{2.71}$$

To compute HHD_h, a base temperature $T_{base} = 15°C$ is adopted; the resulting expression is:

$$HHD_h = max(T_{base} - T_h, 0) \tag{2.72}$$

The total hourly heating degree-hours over the year are then obtained by summing HHD_h across all hours: $HHD_{tot,h} = \sum_1^{8760}(HHD_h)$. Finally, hourly climate-related energy $E_{clime,h}$ is evaluated as follows:

$$E_{clime,h} = (\frac{HHD_h}{HHD_{tot,h}}) \cdot E_{clime,year} \tag{2.73}$$

where $E_{clime,year}$ is the annual climate-driven component of the thermal demand, which consistently with assumption adopted previously correspond to the 75% of the total annual thermal energy demand. Concerning the evaluation of the DHW-use component, it is considered a hourly distribution factor $f_{DHW,h}$ that correspond to the hour of the day [31].

Table 2.4: Hourly distribution factor for domestic hot water (DHW) demand (dimensionless), used to allocate the daily DHW energy demand over the 24 hours of the day.

Hour h	$f_{\mathrm{DHW},h}$
0	0.01
1	0.00
2	0.00
3	0.00
4	0.00
5	0.01
6	0.03
7	0.10
8	0.07
9	0.07
10	0.06
11	0.06
12	0.05
13	0.05
14	0.04
15	0.03
16	0.04
17	0.04
18	0.05
19	0.07
20	0.06
21	0.06
22	0.05
23	0.05
Total	1.00

So the $E_{DHW,h}$ is evaluated as $E_{DHW,h} = f_{DHW,h} \cdot E_{tot,d}$

To evaluate the thermal demand of a single community, a scaling factor is introduced. Since the dataset used refers to the domestic sector at regional level, the demand is downscaled using the number of residential buildings in Catalonua as a proxy. According to the Institut d'Estadística de Catalunya (Idescat), the number of buildings intended for family housing in Catalonia is 1177321 [35]. Assuming one building per community, the corresponding scaling factor is 8.49E-07.

Table 2.5 summarizes the peak and annual electricity demand and the annual thermal demand, which remain constant across all analyzed scenarios.

Max electricity demand	kW	9.2
Annual electricity demand	kWh	54596.72
Total thermal demand	kWh	43476.47

Table 2.5: Summary of electrical and thermal load profile

2.3.2 Hydrogen system dataset

This section presents all the components considered in the hydrogen system, namely the reversible Solid Oxide Cell and the hydrogen tank.

RSOC system dataset

The rSOC system considered in this work is based on the Elcogen elcoStack, in particular the model E3000, characterized by the following features [36] [2]:

Table 2.6: SOEC operating parameters (model E3000).

Parameter	Value
Model	E3000
Power required	3.2 kWh/Nm^3
Hydrogen production rate	3 Nm^3/h
Specific energy consumption	33 kWh/kg
Voltage	143 V to 214 V
Current	60.5 A
Operating temperature	650 °C to 700 °C
Size (W×L×H)	190 × 230 × 280
Weight	33 kg

Table 2.7: SOFC operating parameters (model E3000).

Parameter	Value
Model	E3000 (fuel cell)
Power output	3000 W
Voltage	81 V to 143 V (DC)
Current	0 A to 30 A
Operating temperature	580 °C to 720 °C
Size (W×L×H)	190 × 230 × 280
Weight	33 kg

The SOFC operating points in Table 2.8 are extracted from the manufacturer's SOFC technical data (Table 2.7) [2]:

Table 2.8: SOFC operating points extracted from the SOFC technical data reported in Table 2.7.

Current [A]	Gross efficiency [%]	Power [W]	Voltage [V]
15.0	75.2	1500	100.00
17.5	75.3	1800	102.86
20.0	75.3	2100	105.00
22.5	74.9	2400	106.67
25.0	74.3	2550	102.00
27.5	73.8	2800	101.82
30.0	73.4	3000	100.00

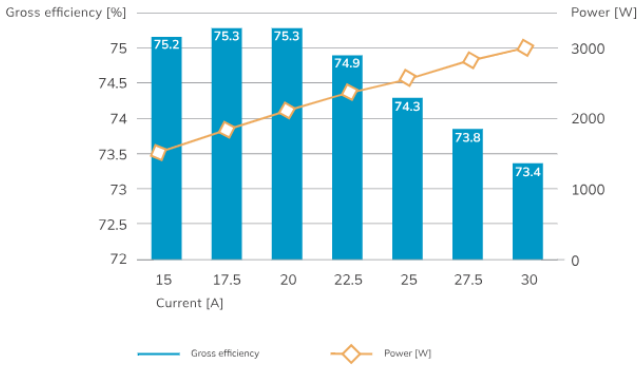

Figure 2.4: Gross efficiency and power as a function of current (SOFC operating points). Reproduced from [2]

To simplify the optimization, the gross efficiency is assumed constant and equal to the average value, set to 74.6%. The source does not specify whether auxiliary consumption is included; therefore, auxiliaries are not modelled explicitly in this work.

Calculation of energy released by the rSOC system

In this case study, the energy exchanged by the rSOC system is evaluated from the reaction enthalpy of the reversible steam electrolysis / fuel-cell process, by deriving the energy content from the stoichiometric hydrogen flow.
The reference reactions are the following [37]:

$$SOEC\ mode: \quad \mathrm{H_2O\,(g)} \longrightarrow \mathrm{H_2\,(g)} + \frac{1}{2}\,\mathrm{O_2\,(g)} \tag{2.74}$$

$$SOFC\ mode: \quad \mathrm{H_2\,(g)} + \frac{1}{2}\,\mathrm{O_2\,(g)} \longrightarrow \mathrm{H_2O\,(g)} \tag{2.75}$$

At standard conditions (25°C), the enthalpy change for water formation in the gas phase is $\Delta H = -241.82\ kJ/mol$ [38]; therefore, the electrolysis reaction has the same magnitude with opposite sign, $\Delta H = +241.82\ kJ/mol$. Kirchhoff's law is used to correct the standard reaction enthalpy from the standard condition temperature $T_1 = 25°C$ to the operating temperature T_2 [39]:

$$\Delta H(T_2) = \Delta H(T_1) + \int_{T_1}^{T_2} \Delta C_p dT \tag{2.76}$$

where $\Delta C_p(T)$ is the difference between the total molar heat capacities (at constant pressure) of products and reactants, weighted by stoichiometric coefficients ν_i, ν_j:

$$\Delta C_p(T) = \sum_i \nu_i C_{p,m,i}^{products}(T) - \sum_j \nu_j C_{p,m,j}^{reactants}(T)\ . \tag{2.77}$$

If ΔC_p is assumed constant over the considered temperature interval, like for this case study, the integral reduces to:

$$\Delta H(T_2) = \Delta H(T_1) + \Delta C_p \cdot (T_2 - T_1)\ . \tag{2.78}$$

The operating conditions are $T = 650°C$ for the SOEC mode [36], while $T = 720°C$ for the SOFC mode [2]. For the SOEC case, $650°C$ is selected as a representative

setpoint at the lower end of the typical SOEC operating window, as shown in Table 2.6. This choice is consistent with operating the electrolyzer in a thermally controlled regime, since SOECs may operate in endothermic, exothermic or thermoneutral conditions depending on the operating voltage relative to the thermoneutral voltage; when operating in endothermal conditions, heat must be supplied to maintain the stack temperature [40]. For the SOFC case, $720°C$ is chosen as a reference condition near the upper end of the reported operating range, as shown in Table 2.7. In general, increasing the operating temperature improves electrolyte ionic conductivity and reduces electrochemical losses, which supports higher cell voltage and performance at a given current density; therefore, a high-temperature reference point is commonly adopted when using manufacturer technical data for performance-based modelling [41]. Constant molar heat capacities are assumed constant as:

- for oxigen $C_{p,O_2} = 29.427\ \frac{j}{mol \cdot K}$ [42]
- for hydrogen $C_{p,H_2} = 28.85\ \frac{j}{mol \cdot K}$ [43]
- for water $C_{p,H_2O} = 33.58\ \frac{j}{mol \cdot K}$ [44]

The resulting enthalpy of reaction is: $\Delta H_{SOEC}(650°C) = +248.06\ \frac{kJ}{mol \cdot K}$ and $\Delta H_{SOFC}(720°C) = -248.76\ \frac{kJ}{mol \cdot K}$
The hydrogen produced/consumed is expressed in moles using the molar mass of molecular hydrogen, $M_{H_2} = 2.016\ \frac{g}{mol}$ [43].
Accordingly, the thermal-equivalent energy associated with the SOEC step is computed as:

$$E_{SOEC}\,[kWh] = m_{H_2,produced}\ [kg] \cdot \frac{1000}{M_{H_2}}\ \left[\frac{mol}{kg}\right] \cdot \Delta H_{SOEC}\ \left[\frac{kJ}{mol}\right] \cdot \frac{1}{3600}\ \left[\frac{kWh}{kJ}\right] \tag{2.79}$$

and, analogously, the energy released in SOFC operation is:

$$E_{SOFC}\,[kWh] = m_{H_2,consumed}\ [kg] \cdot \frac{1000}{M_{H_2}}\ \left[\frac{mol}{kg}\right] \cdot \Delta H_{SOFC}\ \left[\frac{kJ}{mol}\right] \cdot \frac{1}{3600}\ \left[\frac{kWh}{kJ}\right]. \tag{2.80}$$

Because the rSOC periodically switches between electrolysis and fuel-cell operation, a finite transition time is considered. Assuming a 30-minute switching interval in which operation is not fully effective, only 50% of the theoretically produced electrical energy and 50% of the theoretically produced hydrogen are counted as valid contributions during the switch.

Hydrogen tank dataset

The hydrogen tank capacity is an optimization variable; therefore, an upper bound is imposed to reflect practical space limitations. Compressed gaseous hydrogen storage at 350 bar is adopted, a pressure level commonly used in small-to-medium applications [45]. At this pressure, the system volumetric capacity at ambient temperature is taken as $\rho_v = 17.8\ kg_{H_2}/m^3$ [46]. In this work, the maximum available internal storage volume is limited to $V_{max} = 10\ m^3$, that is consistent with a small system. This value leads to a maximum stored hydrogen mass of $m_{H_2,max} = \rho_v \cdot V_{max} = 17.8 \times 10 = 178\ kg$. Accordingly, the hydrogen tank capacity is constrained as $m_{H_2} \leq m_{H_2,max}$.

2.3.3 Thermal Energy Storage (TES) dataset

For the determination of the thermal energy storage (TES) characteristics, the operating temperatures previously assumed for the SOEC and SOFC operation mode are adopted: $650°C$ for the endothermic SOEC process and $720°C$ for SOFC mode.
A phase change material (PCM) is then selected by matching its phase-change temperature to the target operating range of the application, which is a standard criterion in PCM section [8]. In line with approaches commonly used in the literature, where the PCM melting point is chosen close to a representative (often average) operating temperature to maximize effectiveness, a melting temperature near the midpoint of the two operating temperatures is adopted here [47].
The intermediate value between $650°C$ and $720°C$ is $685°C$; therefore, a PCM with a melting point of approximately $685°C$ is selected. This choice places the phase-change temperature about $35°C$ above the SOEC and $35°C$ below the SOFC temperature, providing a balanced margin with respect to both regimes. As a result, the PCM can store and release heat at an almost constant temperature within a range that remains compatible with both operating modes, reducing the risk of premature solidification (if the melting point were too high) or excessive superheating/limited useful latent operation (if it were too low).

The PCM selected to match the target melting temperature is the molten fluoride salt FMgNaK, a eutectic mixture of $(NaF)_{0.345}(KF)_{0.59}(MgF_2)_{0.065}$. Its main thermophysical properties are summarized in Table 2.9 [48, 49].

Table 2.9: Thermophysical properties of the selected PCM.

Property	Numerical value	Unit
Chemical composition	$(NaF)_{0.345}(KF)_{0.59}(MgF_2)_{0.065}$	–
Melting temperature (T_m)	685	°C
Specific heat capacity	1.1 – 1.3	$J\,g^{-1}\,K^{-1}$
Density	2.5 – 2.7	$g\,cm^{-3}$
Thermal expansion coefficient	$(1.5 – 2.0) \times 10^{-4}$	K^{-1}
Viscosity	1.2 – 1.5	mPa s
Thermal stability (max. stable temperature)	> 1000	°C
Toxicity / safety	Moderate	–

In the present work, the TES capacity is constrained by imposing an upper bound on the storage size, like for the hydrogen tank. This choice is motivated by the limited availability of consistent latent-heat (fusion enthalpy) data for FMgNaK, which prevents a fully reliable estimation of the total storage capacity of a latent-heat TES. In general, the total thermal storage capacity of a PCM includes both sensible and latent contribution,

$$E_{TES} = \rho V (C_p \Delta T + L_f) \tag{2.81}$$

where ρ is the PCM density, V the PCM volume, c_p the specific heat capacity, ΔT the operating temperature window and L_f the latent heat of fusion.
Given the lack of validated L_f value for FMgNaK within the considered operating conditions, only the sensible term is used to obtain a conservative estimate of the energy content associated with the selected temperature window,

$$E_{sens} = \rho V C_p \Delta T \ . \tag{2.82}$$

Using the thermophysical properties reported in Table 2.9 and $\Delta T = 70\ K$, this yields approximately 60.7 kWh per 1 m^3 of PCM (sensible contribution only). Therefore, the TES volume is bounded by $V \leq V_{max}$, where V_{max} is considered to be equal to 2 m^3, corresponding to an estimated sensible storage capacity of about 121 kWh.
The latent term is expected to be significant for high-temperature PCM; for instance, a related fluoride/chloride reciprocal salt (NaF-KCl) has been reported with a latent heat up to 454.8 $\frac{J}{g}$ [50]. In order to conservatively account for the latent contribution in the absence of a validated fusion-enthalpy value for FMgNaK, this work assumes

$L_f = 500\ \frac{kJ}{kg}$ as an engineering estimate. Therefore, the adopted TES capacity bound should be interpreted as a practical sizing constraint, rather than an exact measure of the true energy capacity of the latent-heat TES.

2.3.4 Electrical connection and cable sizing

In this work, the electrical connection is represented by a set of lines $\mathscr{L}$ and a discrete catalogue of commercially available cable types $\mathscr{C}$ [51]:

Table 2.10: Discrete catalogue of commercially available cable types used in this work.

S [mm^2]	$I_{\max}$ [A]	R [Ω/km]	Weight [kg/km]
0.75	12	24.000	7.2
1.50	18	12.000	14.4
2.50	25	7.200	24.0
4.00	34	4.500	38.4
6.00	43	3.000	58.0
10.00	59	1.800	96.0
16.00	79	1.125	154.0
25.00	106	0.720	240.0
35.00	129	0.514	336.0
50.00	157	0.360	480.0

For each line $i \in \mathscr{L}$, the model selects exactly one cable type $j \in \mathscr{C}$ by means of a binary decision variable $x_{i,j}$, defined as

$$x_{i,j} = \begin{cases} 1, & \text{if cable type } j \text{ is assigned to line } i, \\ 0, & \text{otherwise.} \end{cases} \tag{2.83}$$

The corresponding "one-cable-per-line" constraint is

$$\sum_{j \in \mathscr{C}} x_{i,j} = 1 \quad \forall i \in \mathscr{L} \ . \tag{2.84}$$

Each line i is characterized by a required maximum current $I_i^{req}\,[A]$ and a length $l_i\,[km]$. Each cable type j is described by its ampacity $I_j^{max}\,[A]$, its linear weight $w_j\left[\frac{kg}{km}\right]$, and a unit purchase cost $c_j^{kg}\left[\frac{€}{kg}\right]$. To avoid excessive oversizing, cable selection is constrained so that the ampacity of the selected cables does not exceed a fixed margin above the required current. While cable ampacity is commonly selected with a 25% margin citazione, the present formulation adopts an oversizing capacity of 50%. This higher threshold accounts for uncertainties and operating deviations while still preventing unjustifiable oversizing:

$$\sum_{j\in\mathscr{C}} x_{i,j} I_j^{max} \cdot 1.5 \leq I_i^{req} \quad \forall i \in \mathscr{L}\ . \tag{2.85}$$

2.3.5 Components cost data

This subsection summarizes the cost assumptions adopted in the analysis and introduces the reference prices used for each component. The overall project lifetime is set to 30 year and a real discount rate of 5% is assumed.

PV cost data

As stated in the previous subsection Optimization model in General formulation, the PV system is treated as a pre-existing asset; therefore, its CAPEX cost is excluded. However, to estimate PV fixed OPEX and replacement costs, a reference CAPEX of 800 $€/kW_{installed}$ is assumed, consistent with the specific investment costs reported for Spain [52]. Fixed operating and maintenance costs (OPEX) is set to 1% of this reference CAPEX per year , which lies within the 0.5-1.5% range commonly reported for PV OPEX [53]. To account for PV component replacements over the lifetime, an aggregate replacement cost equal to 30% of the reference CAPEX is assumed [54]. PV lifetime is assumed equal to 25 years, consistent with commonly adopted PV module useful-life assumptions in the literature [55].

Hydrogen system cost data

The rSOC specific investment cost is first taken from the literature as a baseline value of 5000 €/kW [56]. In this work, however, the rSOC is assumed to rely on an

advanced anode-supported-cell technology for which a substantial manufacturing-driven cost reduction is reported; accordingly, the rSOC CAPEX is reduced by 60% with respect to the baseline, resulting in an assumed CAPEX of 2000 €/kW [54].
A stack lifetime of 8 years is assumed, consistent with published durability ranges for solid oxide technology of 5-10 years (i.e., 40,000-80,000 operating hours) [57].
A replacement cost equal to 45% of the adopted CAPEX is assumed to account for stack replacement and major interventions on auxiliary components (assumption).
Fixed annual OPEX it is assumed equal to 12% of the reduced CAPEX. This choice is intended to avoid unrealistically low operating costs obtained by scaling OPEX proportionally with stack manufacturing cost reductions, since a substantial share of operation and maintenance activities concerns balance-of-plant subsystems and associated services rather than the stack alone [58]. For consistency, both fixed annual OPEX and replacement expenditures are therefore parametrized as fractions of the adopted rSOC CAPEX. Although CAPEX is reduced to reflect the assumed technology learning, these fractions are kept deliberately conservative to account for balance-of-plant maintenance and major interventions that may not scale proportionally with stack cost reductions (assumption).
Cell degradation is not modeled as a separate monetary term; instead, it is implicitly accounted for through the assumed component lifetime and through the fixed OPEX.

Concerning the hydrogen tank, its CAPEX is reported in the range 30-40 \$/kWh in the reversible SOFC system study [59]. In this work, a mid-range value of 35 \$/kWh is adopted and converted in € per kg_{H_2} using an exchange rate of 1 \$ = 0.85 € (assumed average over 2025-2026) [60], the energy conversion 1 $kWh = 3.6\ MJ$, and the hydrogen lower heating value $LHV_{H_2} \approx 120\ MJ/kg$.
Accordingly, the specific tank CAPEX becomes:

$$c_{tank}^{capex} = 35\frac{\$}{kWh} \cdot 0.85\frac{€}{\$} \cdot \frac{1}{3.6}\frac{kWh}{MJ} \cdot 120\frac{MJ}{kg_{H_2}} \approx 9.92 \times 10^2 \frac{€}{kg_{H_2}} . \tag{2.86}$$

The lifetime of the hydrogen tank is assumed to be 20 years, and both the replacement cost and fixed OPEX are modeled as a fractions of the CAPEX, 45% and 1% respectively, consistently with the rSOC system.

Thermal energy storage cost data

The cost of a high-temperature PCM thermal storage unit is reported to be 60 €/kWh [8]. In this work, this value is adopted as a conservative estimate, intended to represent not only the PCM material but also the overall storage system. The PCM storage lifetime is assumed to be 20 years. Replacement cost and fixed annual OPEX are modeled as fractions of the PCM storage CAPEX, equal to 30% and 1% per year, respectively (assumption).

Cable cost data

Cable costs are estimated from the copper content, assuming a copper base price of 150 € per 100 kg of Cu [61]. The cable lifetime is assumed to be 25 years . Replacement costs and fixed annual OPEX are modeled as fractions of the cable CAPEX, equal to 30% and 1% per year, respectively (assumption).

2.3.6 Price of energy

Daily energy price data are collected from official Iberian market transparency platforms. Electricity prices (€/MWh) correspond to the Spanish day-ahed spot market daily price series published on ESIOS (Red Eléctrica de España), indicator "Precio mercado SPOT Diario España" [62]. Natural gas price (€/MWh) are taken from MIBGAS "Price and volume index per gas day" (daily price index) [63]. The electricity and gas series cover different time windows (electricity : 2024; gas : 2024-2025), due to data availability. In Table 2.11 are shown the maximum, minimum and average values of the hourly prices considered.

Table 2.11: Maximum, Minimum and Average values for Hourly Electricity and Gas Prices

	Electricity [€/MWh]	Gas [€/MWh]
Maximum	193.00	57.05
Minimum	−2.00	26.74
Average	63.03	36.75

2.4 Scenarios

Since the actual installed PV capacity for the case study is not available, a scenario-based approach was adopted to test the sensitivity of the results to different PV sizes. As a baseline, we assumed 6 kWp installed per community, as this represents a realistic small-to-medium rooftop system and is broadly consistent with typical residential-scale power levels in Spain [64].
Three PV installation scenarios are therefore considered:

- Scenario 1: 6 kWp per community (12 kWp total),
- Scenario 2: an intermediate case with asymmetric capacities, assuming 6 kWp in one community and 12 kWp in the other (18 kWp total),
- Scenario 3: 12 kWp per community (24 kWp total).

In addition to the PV-size sensitivity analysis, a sensitivity study on the optimization weights is performed. As described in Section 2.2.2, the model includes two main objective functions: one based on economic cost (electricity price) and one based on environmental impact (carbon footprint).

The optimization is first run in single-objective mode, i.e., minimizing the cost objective while excluding the carbon-footprint objective, and then minimizing the carbon-footprint objective while excluding the cost objective. Finally, a weighted formulation is adopted, starting from equal weights (0.5 for cost and 0.5 for carbon footprint) and progressively increasing the weight assigned to the carbon-footprint term up to 0.9, with the cost weight decreasing accordingly to 0.1.

Chapter 3

Results

This chapter presents the results obtained from the optimization simulations described in Chapter 2. The aim is to report the model outputs in a clear and reproducible way. The discussion and interpretation of the observed trends are intentionally deferred to Chapter 4.

The results are organized according to the three PV installation scenarios considered in the study, in order to evaluate the sensitivity of the results to different installed capacities. For each scenario, the outcomes obtained under cost-oriented, carbon-oriented and weighted multi-objective formulations are reported.

Due to the large volume of data generated, this chapter summarizes the most significant findings and performance indicators. The complete set of detailed numerical results for all simulated cases is provided in Appendix B for further reference.

3.1 Scenario 1: 12 kWp total installed PV capacity

The first scenario analyzes the impact of a total PV installed capacity of 12 kWp. This configuration represents the minimum capacity considered in this study. Table B.1 summarizes the overall PV production characteristics.

Table 3.1: Photovoltaic generation summary for the 12 kWp scenario

Parameter	Unit	Value
Max PV forecast	kW	10.35
Total PV overproduction	kWh	25516.97
Timestep with surplus PV production	–	1276

The overall results of the analysis are presented here, highlighting the most relevant values and performance indicators.
The plots are shown as a function of the weight assigned to cost minimization, w_{cost}.

As illustrated in Figure 3.1, the Net Present Cost (NPC) and of the initial investment follow similar trend. When full priority is assigned to emission reduction, both values rise dramatically, increasing by approximately 3 to 4 times compared to the cases in which weight is also assigned to the system cost. The exact numerical results are reported in Table 3.2.

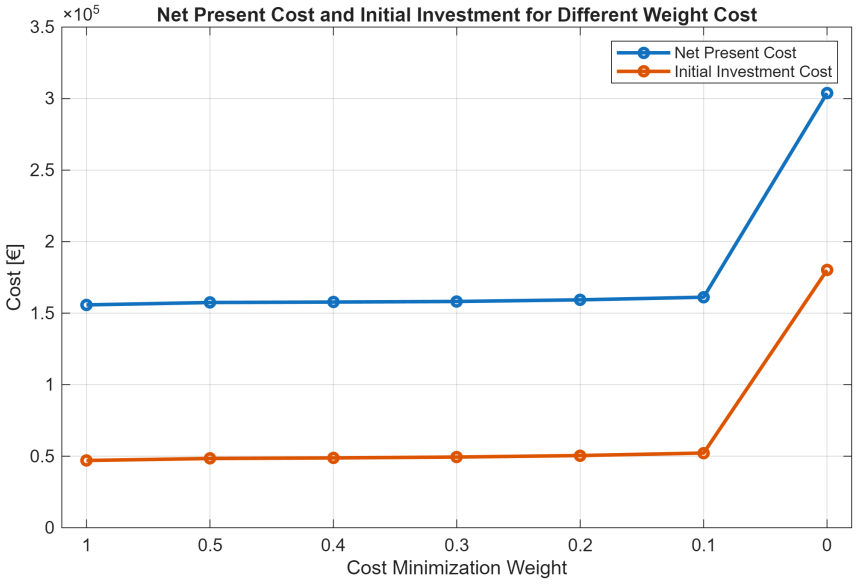

Figure 3.1: Net Present Cost and Initial Investment for Different Weight Cost, Scenario 12 kWp installed

Table 3.2: Net Present Cost and Initial Investment for Different Cost Weights in the 12 kWp Scenario

Parameter [€]	w_{cost}						
	1	**0.5**	**0.4**	**0.3**	**0.2**	**0.1**	**0**
Net Present Cost	155781.30	157447.23	157763.57	158180.60	159317.96	161151.02	303786.38
Initial Investment	47018.37	48401.96	48803.09	49412.41	50459.19	52226.07	180080.12

The payback time is not defined because the additional investment is not recovered over the analysis period with respect to the reference case. The reference case represents the baseline configuration without the planned system; therefore, the electricity demand that is not covered by PV generation is purchased from the grid, while the gas demand is entirely met through natural gas purchase.
Figures 3.2 and 3.3 report the values of the annual system cost and the corresponding relative percentage loss. Tables 3.3 reports the exact numerical values.

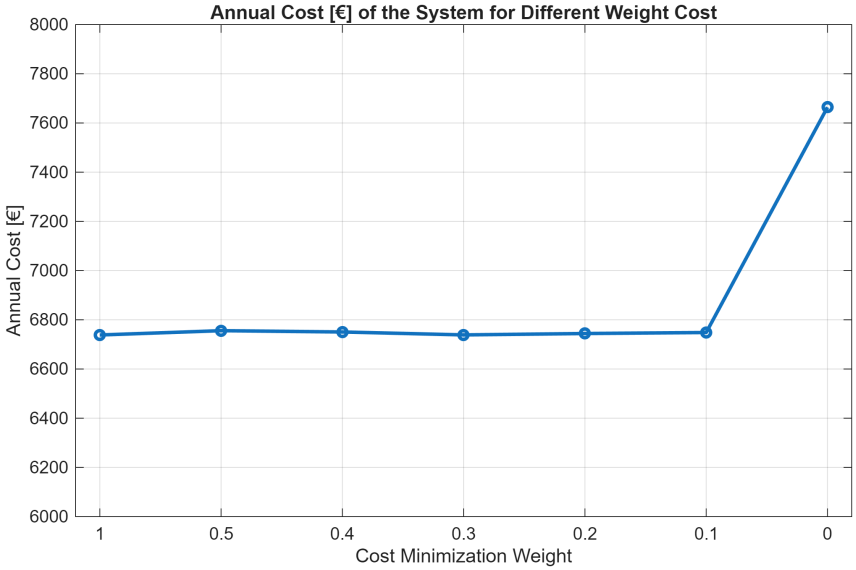

Figure 3.2: Annual Cost of the System for Different Weight Cost, Scenario 12 kWp installed

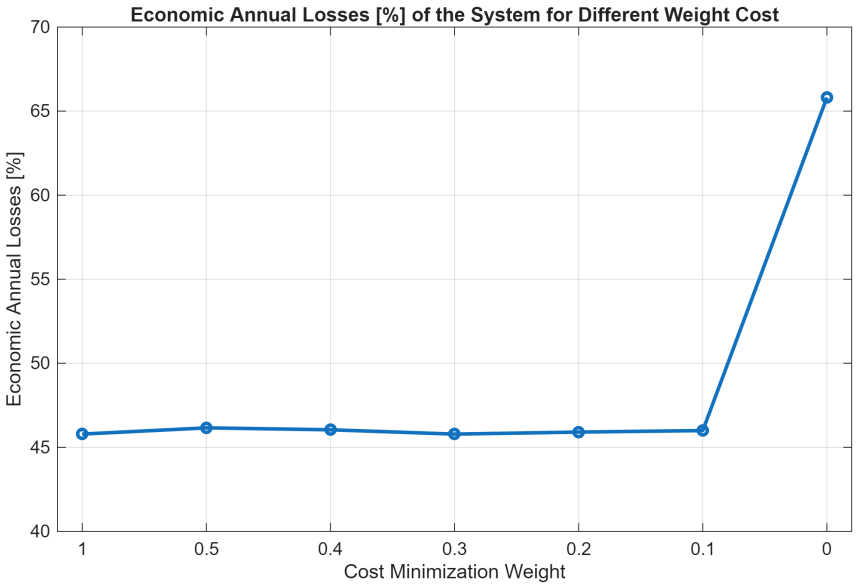

Figure 3.3: Economic Annual Losses [%] with respect to the Reference Case for Different Weight Cost, Scenario 12 kWp installed

Table 3.3: Annual Cost and Percentage Economic Annual Losses for Different Cost Weights in the 12 kWp Scenario

Parameter	w_{cost}						
	1	**0.5**	**0.4**	**0.3**	**0.2**	**0.1**	**0**
Annual Cost [€]	6738.27	6755.76	6750.51	6738.60	6744.21	6748.31	7664.07
Economic Annual Losses [%]	45.79	46.16	46.04	45.79	45.91	46.00	65.81

The maximum amount of H_2 stocked corresponds to the hydrogen tank capacity. Figure 3.4 illustrates the increase of the stored hydrogen as greater priority is assigned to emission reduction, while figure 3.5 reports the corresponding values of the percentage emission reduction. The exact values are shown in Table 3.4.

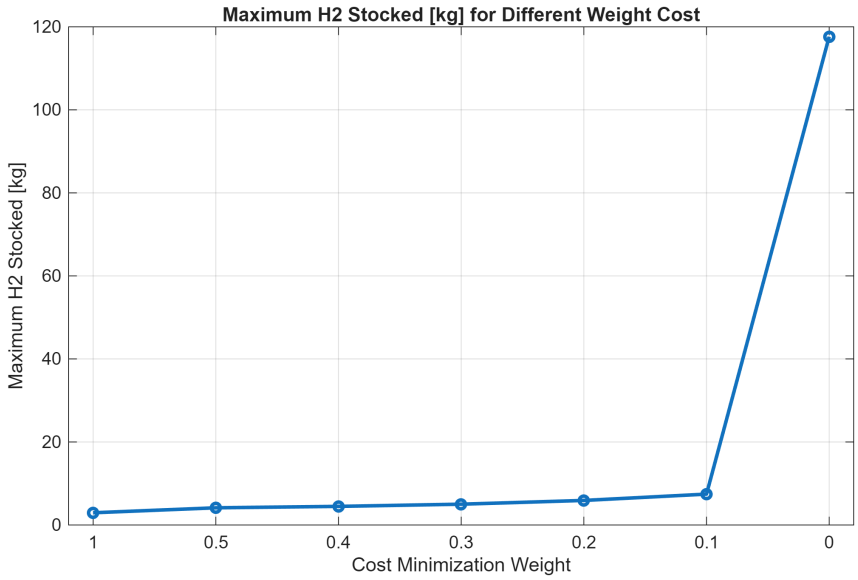

Figure 3.4: Hydrogen Tank Capacity [kg] for Different Weight Cost, Scenario 12 kWp installed

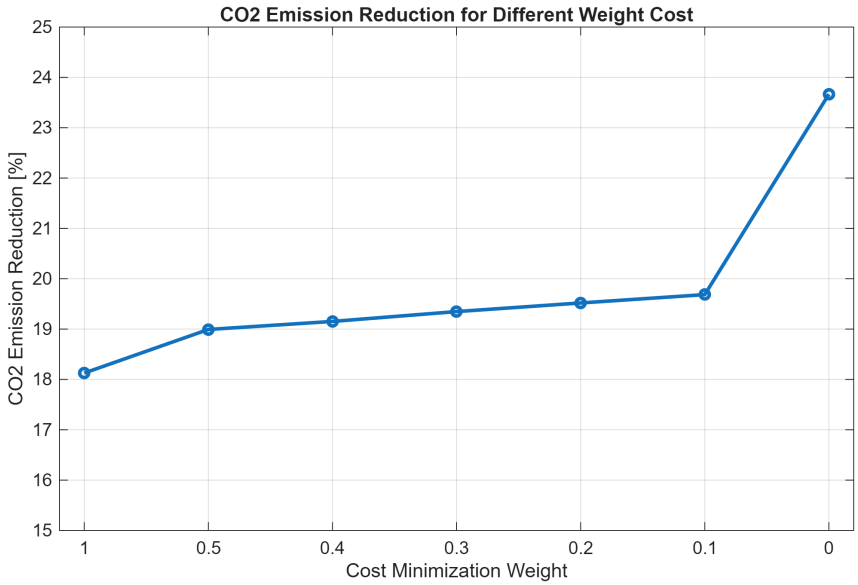

Figure 3.5: CO_2 Emission Reduction [%] with respect to the Reference Case for Different Weight Cost, Scenario 12 kWp installed

Table 3.4: Capacity of Hydrogen Tank [kg] and CO_2 Emission Reduction [%] for Different Cost Weights in the 12 kWp Scenario

Parameter	w_{cost}						
	1	**0.5**	**0.4**	**0.3**	**0.2**	**0.1**	**0**
Hydrogen Tank Capacity [kg]	2.95	4.14	4.48	5.01	5.91	7.44	117.63
CO_2 Emission Reduction [%]	18.13	18.99	19.15	19.35	19.52	19.68	23.67

An important trend to highlight is the amount of electricity purchased, which decreases as w_{cost} decreases, as illustrated in Figure 3.6:

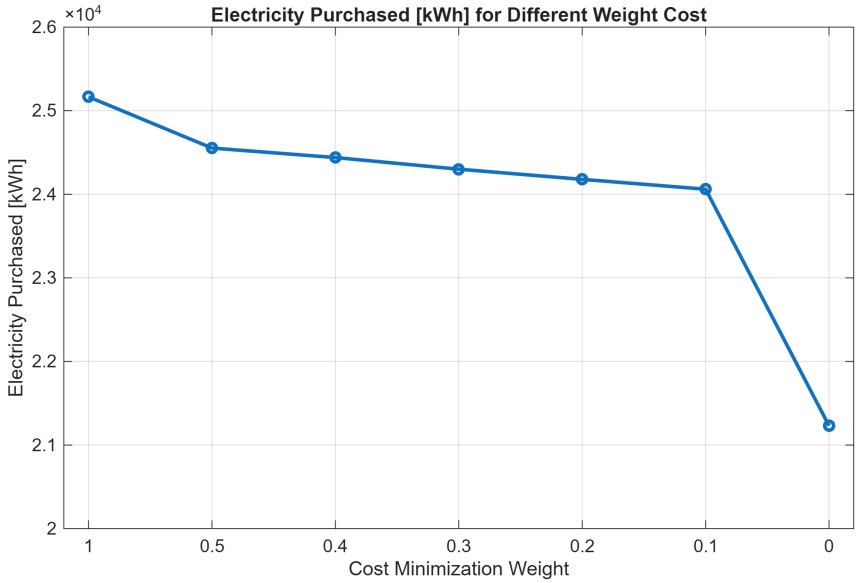

Figure 3.6: Total Amount of Electricity Purchased for Different Weight Cost, Scenario 12 kWp installed

With regard to the thermal balance, all simulations resulted in a TES capacity equal to 0 kWh, as the amount of recoverable heat is insufficient to make thermal storage cost-effective. It is therefore important to analyze the heat exchanges taking place within the rSOC system. In SOEC mode, the stack requires an initial thermal input - supplied by purchased gas via district heating - to reach its operating temperature. However, once the SOEC mode has drawn the initial thermal input, the subsequent switch to SOFC operation generates enough heat to cover the thermal

needs of the following cycles. As a result, gas is only required during initial heating phase, after which the heat produced in SOFC mode is largely sufficient to be reused, without the need for further gas purchases. Table 3.5 shows the values of the total thermal energy exchanged between the two modes throughout the year.

Table 3.5: Thermal Energy Exchanged in the rSOC for Different Cost Weights in the 12 kWp Scenario

Parameter [kWh]	w_{cost}						
	1	**0.5**	**0.4**	**0.3**	**0.2**	**0.1**	**0**
Heat produced by rSOC (SOFC)	17761.95	18610.95	18767.40	18959.19	19126.88	19289.17	23190.55
Heat absorbed by rSOC (SOEC)	-17711.96	-18558.58	-18714.59	-18905.84	-19073.06	-19234.90	-23125.29

3.2 Scenario 2: 18 kWp total installed PV capacity

The second scenario examines the impact of a total PV installed capacity of 18 kWp; the common PV production characteristics are illustrated in Table B.5.

Table 3.6: Photovoltaic generation summary for the 18 kWp scenario

Parameter	**Unit**	**Value**
Max PV forecast	kW	15.53
Total PV overproduction	kWh	30209.03
Timestep with surplus PV production	–	2111

Figure 3.7 highlights a similar pattern for the Net Present Cost (NPC) and of the initial investment. When emission reduction is full prioritized an increase of approximately 3 to 4 times is seen, as it happened for the first scenario in Section 3.1. The exact numerical results are reported in Table 3.7.

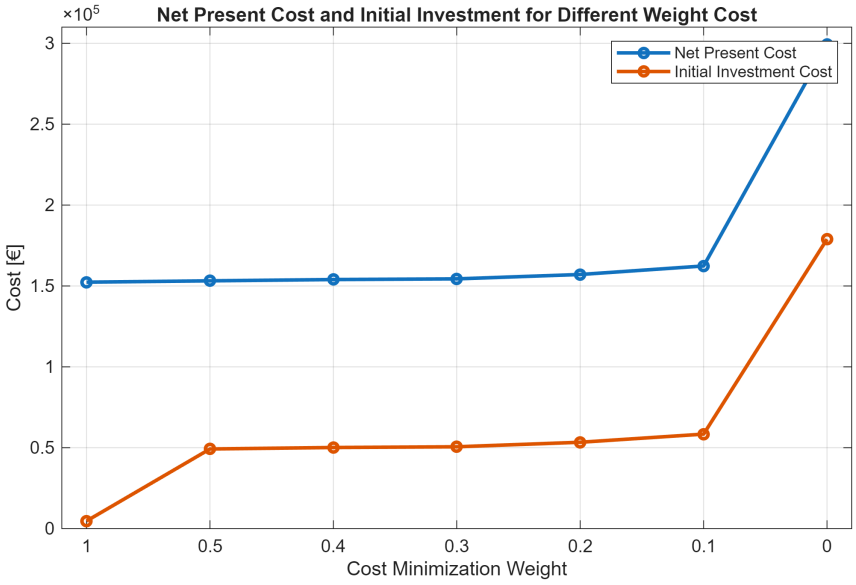

Figure 3.7: Net Present Cost and Initial Investment for Different Weight Cost, Scenario 18 kWp installed

Table 3.7: Net Present Cost and Initial Investment for Different Cost Weights in the 18 kWp Scenario

Parameter [€]	w_{cost}						
	1	**0.5**	**0.4**	**0.3**	**0.2**	**0.1**	**0**
Net Present Cost	152342.77	153176.20	153959.12	154384.56	157088.70	162359.31	299243.74
Initial Investment	4729.76	49243.28	50151.79	50602.07	53392.22	58425.52	178921.14

The payback time cannot be determined because the additional investment is not recovered within the analysis period relative to the reference case.
Figures 3.8 and 3.9 report the values of the annual system cost and the corresponding relative percentage loss. Tables 3.8 reports the exact numerical values.

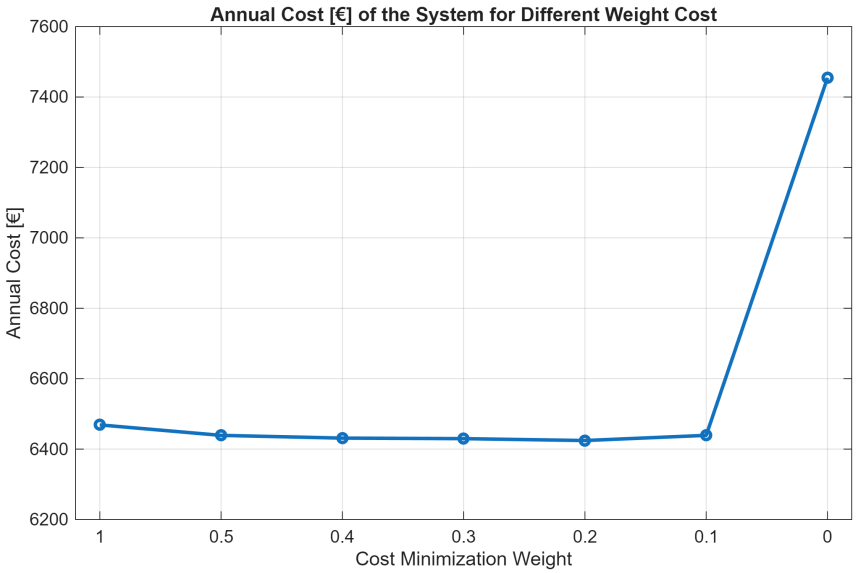

Figure 3.8: Annual Cost of the System for Different Weight Cost, Scenario 18 kWp installed

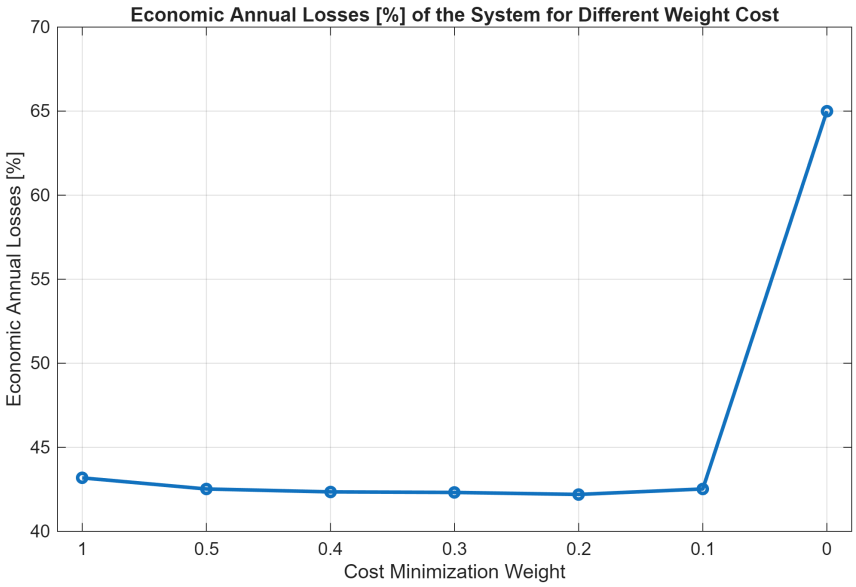

Figure 3.9: Economic Annual Losses [%] with respect to the Reference Case for Different Weight Cost, Scenario 18 kWp installed

Table 3.8: Annual Cost and Percentage Economic Annual Losses for Different Cost Weights in the 18 kWp Scenario

Parameter	w_{cost}						
	1	**0.5**	**0.4**	**0.3**	**0.2**	**0.1**	**0**
Annual Cost [€]	6468.78	6439.03	6431.25	6429.71	6424.39	6439.09	7454.44
Economic Annual Losses [%]	43.18	42.52	42.35	42.32	42.20	46.52	65.00

The maximum amount of H_2 stocked corresponds to the hydrogen tank capacity, it is shown in Figure 3.10. Figure 3.11 reports the corresponding values of the percentage emission reduction. The exact values are shown in Table 3.9.

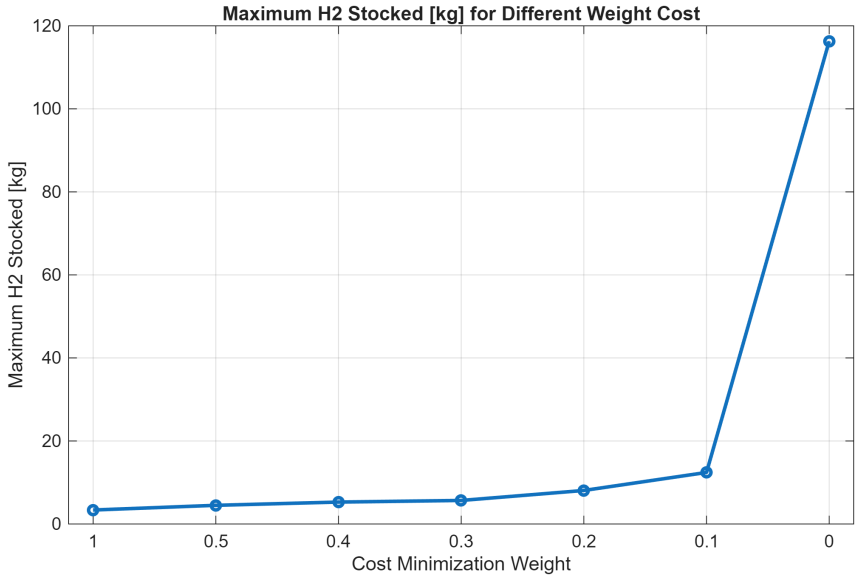

Figure 3.10: Hydrogen Tank Capacity [kg] for Different Weight Cost, Scenario 18 kWp installed

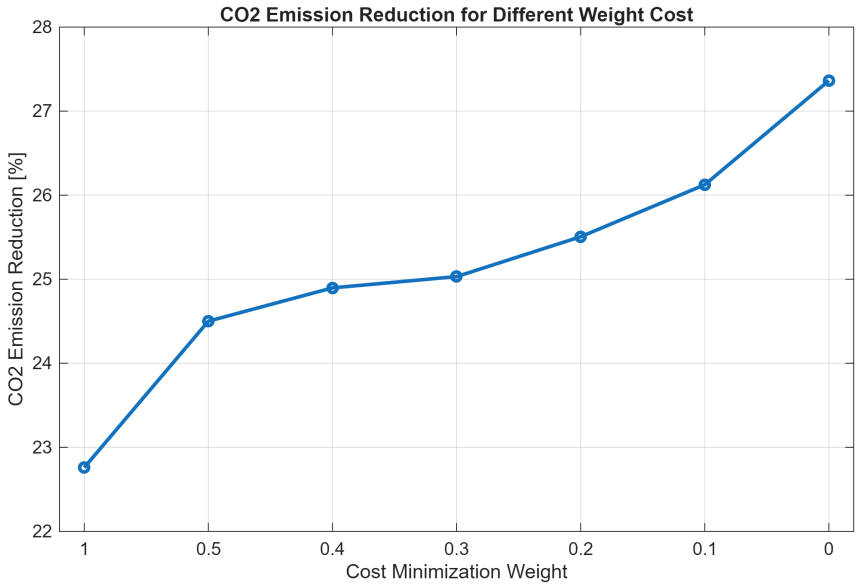

Figure 3.11: CO_2 Emission Reduction [%] with respect to the Reference Case for Different Weight Cost, Scenario 18 kWp installed

Table 3.9: Capacity of Hydrogen Tank [kg] and CO_2 Emission Reduction [%] for Different Cost Weights in the 18 kWp Scenario

Parameter	w_{cost}						
	1	**0.5**	**0.4**	**0.3**	**0.2**	**0.1**	**0**
Hydrogen Tank Capacity [kg]	3.36	4.5	5.28	5.67	8.07	12.41	116.29
CO_2 Emission Reduction [%]	22.76	24.50	24.90	25.03	25.51	26.12	27.36

The amount of electricity purchased decreases as w_{cost} decreases. It is illustrated in Figure 3.12:

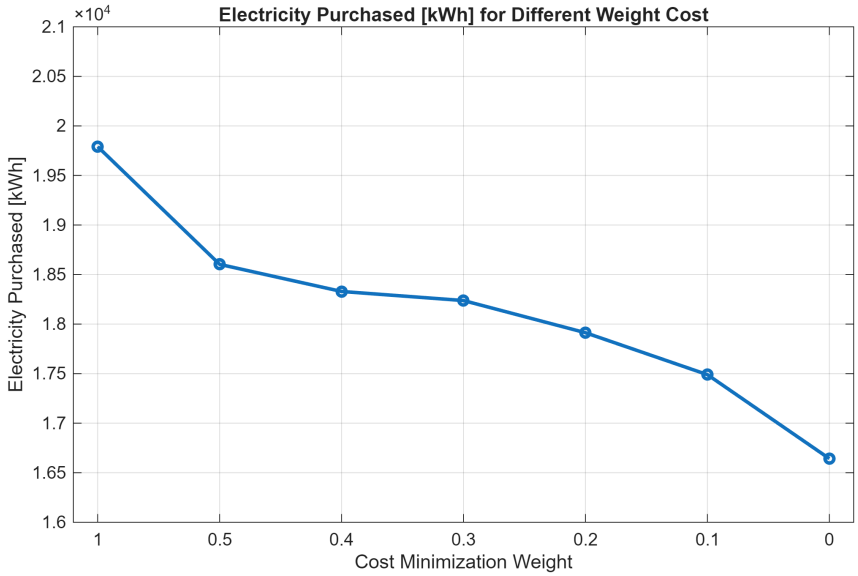

Figure 3.12: Total Amount of Electricity Purchased for Different Weight Cost, Scenario 18 kWp installed

Regarding the thermal balance, all simulations resulted in a TES capacity equal to 0 kWh, for the same reasons discussed in Scenario 1 in Section 3.1. The heat exchanges occurring within the rSOC therefore follow an analogous behavior: gas is purchased exclusively during the initial heating phase of SOEC operation, after which the heat recovered from SOFC mode is sufficient to cover the thermal needs of the subsequent cycles. Table 3.10 reports the total thermal energy exchanged between the two operating modes.

Table 3.10: Thermal Energy Exchanged in the rSOC for Different Cost Weights in the 18 kWp Scenario

Parameter [kWh]	w_{cost}						
	1	**0.5**	**0.4**	**0.3**	**0.2**	**0.1**	**0**
Heat produced by rSOC (SOFC)	21459.02	23097.66	23474.61	23534.47	24048.40	24631.75	25799.87
Heat absorbed by rSOC (SOEC)	-21398.64	-23032.66	-23408.56	-23534.47	-23980.73	-24562.43	-25727.27

3.3 Scenario 3: 24 kWp total installed PV capacity

The last scenario investigates the impact of a total PV installed capacity of 24 kWp, that is the higher installed capacity considered in this work. The common PV production characteristics are illustrated in Table B.9.

Table 3.11: Photovoltaic generation summary for the 24 kWp scenario

Parameter	Unit	Value
Max PV forecast	kW	20.7
Total PV overproduction	kWh	49239.85
Timestep with surplus PV production	–	2462

The Net Present Cost (NPC) and of the initial investment trends are illustrated in Figure 3.13. When emission reduction is full prioritized an increase of approximately 3 to 4 times is seen. The exact numerical results are reported in Table 3.12.

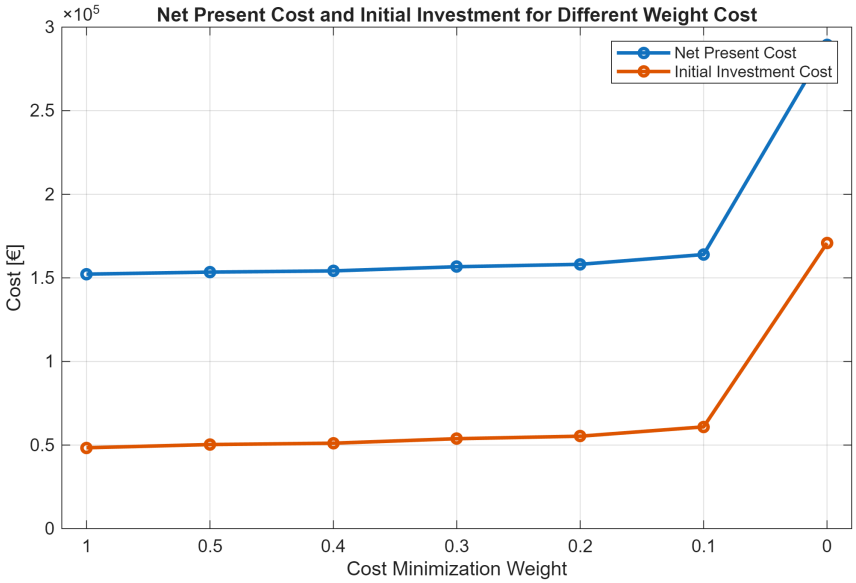

Figure 3.13: Net Present Cost and Initial Investment for Different Weight Cost, Scenario 24 kWp installed

Table 3.12: Net Present Cost and Initial Investment for Different Cost Weights in the 24 kWp Scenario

Parameter [€]	w_{cost}						
	1	**0.5**	**0.4**	**0.3**	**0.2**	**0.1**	**0**
Net Present Cost	152233.82	153461.45	154177.22	156666.17	158103.54	163959.00	289450.45
Initial Investment	48377.40	50304.79	51112.57	53800.50	55296.86	60878.93	170805.81

Since the additional investment is not recovered, the payback time is not evaluated.

Figures 3.14 and 3.15 report the values of the annual system cost and the corresponding relative percentage loss. Tables 3.13 reports the exact numerical values.

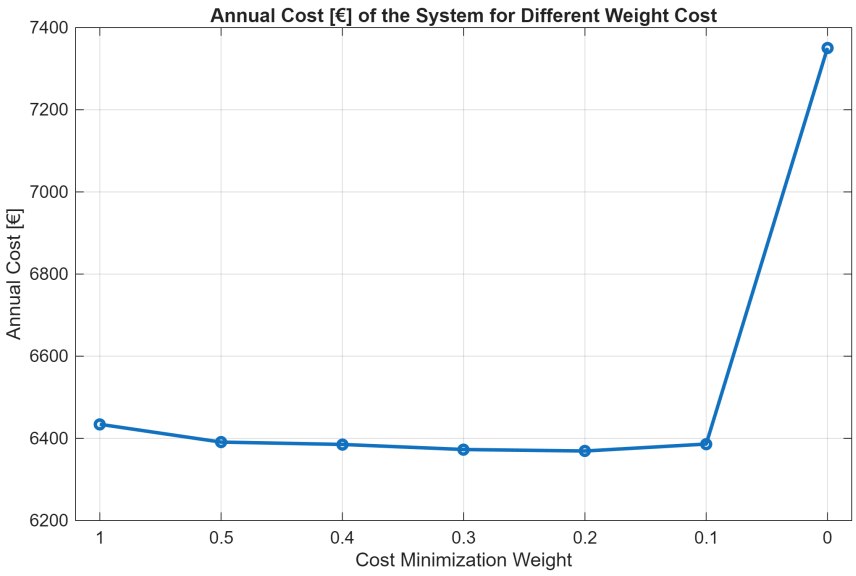

Figure 3.14: Annual Cost of the System for Different Weight Cost, Scenario 24 kWp installed

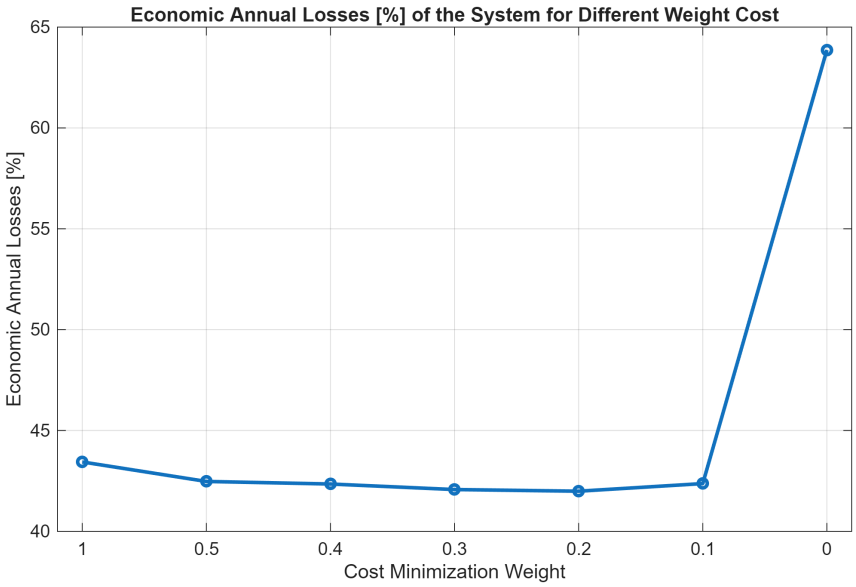

Figure 3.15: Economic Annual Losses [%] with respect to the Reference Case for Different Weight Cost, Scenario 24 kWp installed

Table 3.13: Annual Cost and Percentage Economic Annual Losses for Different Cost Weights in the 24 kWp Scenario

Parameter	w_{cost}						
	1	**0.5**	**0.4**	**0.3**	**0.2**	**0.1**	**0**
Annual Cost [€]	6434.29	6390.94	6385.24	6372.91	6369.26	6386.20	7350.48
Economic Annual Losses [%]	43.44	42.47	42.35	42.07	41.99	42.37	63.87

Figure 3.16 reports the hydrogen tank capacity, that corresponds to the maximum amount if hydrogen stocked. The corresponding values of the percentage emission reduction is in Figure 3.17. The exact values are shown in Table 3.14.

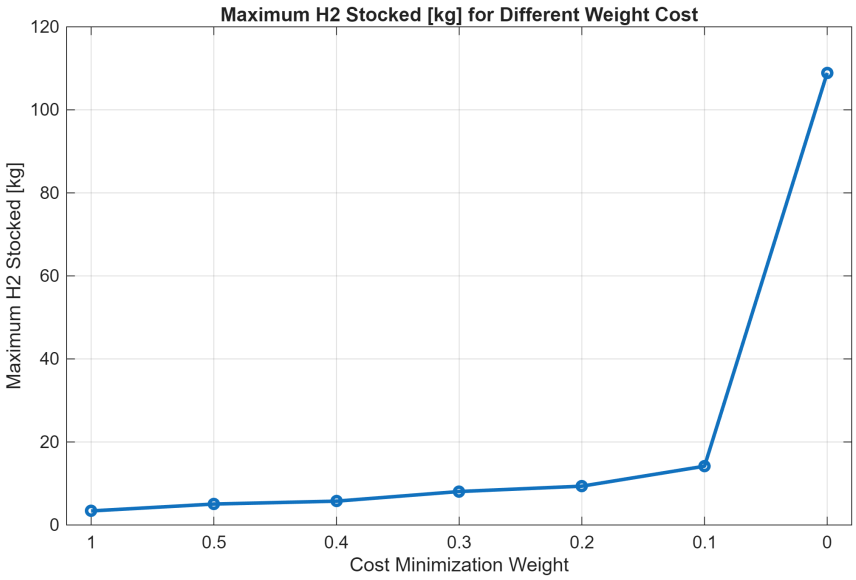

Figure 3.16: Hydrogen Tank Capacity [kg] for Different Weight Cost, Scenario 24 kWp installed

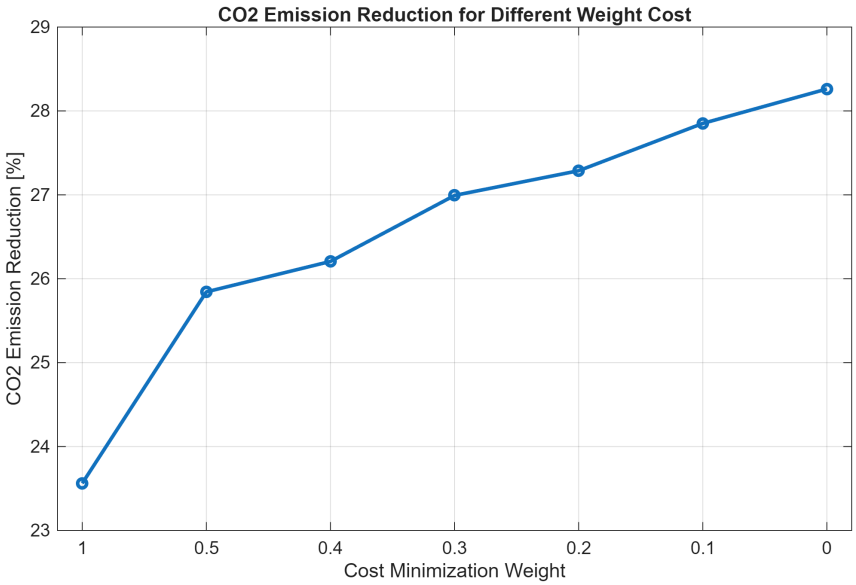

Figure 3.17: CO_2 Emission Reduction [%] with respect to the Reference Case for Different Weight Cost, Scenario 24 kWp installed

Table 3.14: Capacity of Hydrogen Tank [kg] and CO_2 Emission Reduction [%] for Different Cost Weights in the 24 kWp Scenario

Parameter	w_{cost}						
	1	**0.5**	**0.4**	**0.3**	**0.2**	**0.1**	**0**
Hydrogen Tank Capacity [kg]	3.38	5.05	5.74	8.06	9.35	14.16	108.91
CO_2 Emission Reduction [%]	23.56	25.84	26.21	26.99	27.29	27.85	28.26

The amount of electricity purchased decreases as w_{cost} decreases. It is illustrated in Figure 3.18:

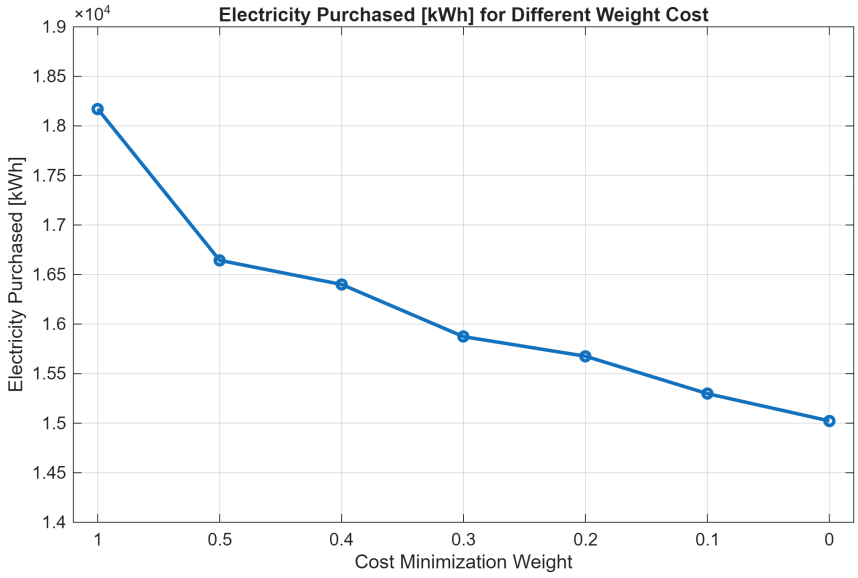

Figure 3.18: Total Amount of Electricity Purchased for Different Weight Cost, Scenario 24 kWp installed

From the thermal balance perspective, all simulations resulted in a TES capacity equal to 0 kWh. Consequently, the heat exchanges within the rSOC deserve particular attention, since the thermal demand is supplied almost entirely by purchased gas. Table 3.15 reports the total thermal energy exchanged between the two operating modes.

Table 3.15: Thermal Energy Exchanged in the rSOC for Different Cost Weights in the 24 kWp Scenario

Parameter [kWh]	w_{cost}						
	1	**0.5**	**0.4**	**0.3**	**0.2**	**0.1**	**0**
Heat produced by rSOC (SOFC)	21762.84	23870.38	24205.47	24932.08	25204.18	25724.76	26103.96
Heat absorbed by rSOC (SOEC)	-21701.60	-23803.21	-24137.36	-24861.92	-25133.26	-25652.37	-26030.51

Chapter 4

Discussion

This chapter discusses the results presented in Chapter 3, interpreting them in relation to the aim of the study.
The discussion is organized into six main sections. First, the economic implications of the findings are examined, followed by hydrogen-related considerations, emission and environmental implications and thermal considerations. The chapter then addresses the limitations of the analysis and concludes with possible future developments.

4.1 Economic implications

All the simulated cases, considering both the different objective functions and the different installed PV scenarios, result in an economic loss when compared with the reference case in which electricity is purchased directly from the grid and natural gas supplied by the gas network. This outcome is observed even though the analysis assumes a lower CAPEX than current market values, as discussed in Subsection 2.3.5. Within the price framework considered in this work, presented in Subsection 2.3.5, the proposed system remains economically less favorable than directly purchasing electricity and gas from external supply networks. The main reason is that, despite the reduced CAPEX assumed in the model, the investment cost of the system is still too high to make it competitive under current energy prices. In addition, the hydrogen tank represents a significant share of the total CAPEX, since its cost increases substantially when hydrogen production becomes larger. More generally, this capital

cost should not be interpreted as limited to the core electrochemical unit alone, but as including the full system configuration and installation requirements associated with solid oxide technologies, such as equipment supply, installation, civil works, electrical infrastructure and balance-of-plant components [65]. The OPEX associated with the rSOC is also kept relatively high compared with the CAPEX assumptions, as explained in Subsection 2.3.5. This is consistent with the current state of solid oxide technologies, for which operating costs are influenced not only by maintenance needs, but also by downtime, standby operation, and auxiliary system such as heating, compression, purification and cooling [65]. In addition, replacement costs remain relevant, in particular because stack degradation and component failure may require the substitution or serving of stacks over the system lifetime [65]. Overall, economic viability is still strongly affected by high investment and operating costs, as they remain relatively immature and not yet widely deployed at commercial scale [66]. This is also consistent with the current development stage of solid oxide technologies. As these systems move from early deployment to wider industrial adoption, their costs are expected to decrease not only because of lower capital costs, but also due to learning-by-doing, economies of scale, design standardization, and improvements in component durability and system lifetime. In this sense, the reduction in operating and replacement costs is not only a consequence of larger market diffusion itself, but also of the technological improvements that diffusion enables, such as lower degradation, higher reliability and lower maintenance needs [67, 68].

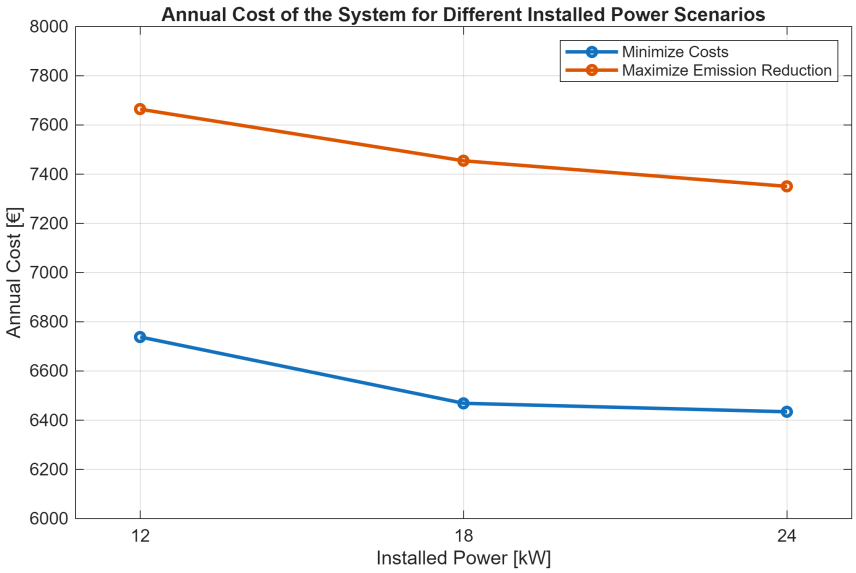

Figure 4.1: Annual Cost of the System for Different Installed Power Scenarios

The annual costs are now analyzed as a function of the installed PV capacity, in Figure 4.1. For clarity, the plot only reports the two extreme optimization cases, since the intermediate cases exhibit the same overall trend. This choice improves the readability of the figures while preserving the interpretation of the results. The annual system cost decreases as the installed PV capacity increases. This reduction is mainly driven by the lower amount of electricity that must be purchased from the grid. As Figure 4.2 shows, as the PV capacity increases, electricity purchase decreases and a larger share of the electrical demand is directly covered by on-site generation, while the additional surplus electricity can be covered into hydrogen and later reused within the system (see Section 4.2). Therefore, increasing the installed PV capacity reduces both direct dependence on grid electricity and the need for external energy supply, leading to lower annual operating costs.

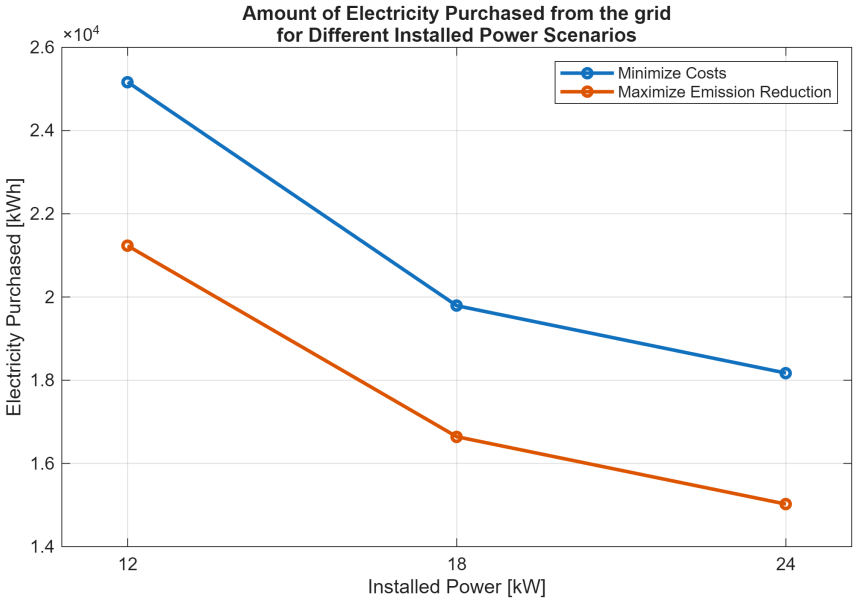

Figure 4.2: Annual Amount of Electricity Purchased from the Grid for Different Installed Power Scenarios

The trend of the percentage economic losses follows the same of logic of the annual cost of the system, as expected. The values are illustrated in Table 4.1.

Table 4.1: Economic Annual Losses [%] for Different Installed Power Scenarios

	12 kW	18 kW	24 kW
Minimization of Total Cost	45.79	43.18	43.44
Maximization of Emission Reduction	65.81	65.00	63.87

A slight deviation from the overall trend can be observed for the 18 kW case. This intermediate configuration represents a transition point in the system design, where the balance between grid electricity purchases, PV surplus exploitation, hydrogen production, and component sizing differs from both the 12 kW and 24 kW scenarios. As a result, the corresponding economic indicator does not follow a perfectly monotonic trend, but rather reflects the local trade-off identified by the optimization process.

Table 4.2: Total Investment Cost [€] for Different Installed Power Scenarios

	12 kW	18 kW	24 kW
Minimization of Total Cost	47 018.37	47 929.76	48 377.40
Maximization of Emission Reduction	180 080.12	178 921.14	170 805.81

Table 4.2 shows the total investment cost as a function of the installed PV capacity for the two extreme optimization objectives. Under the cost-minimization objective, the investment cost exhibits a slight increase as the installed PV capacity rises. By contrast, under the emission-minimization objective, the investment cost decreases with increasing PV capacity.

In the cost-minimization case, this behavior can be explained by the structure of the optimization objective itself. Since the model aims to minimize the total system cost, it selects the lower-capex configuration compatible with system operation for each PV size. However, when the installed PV capacity increases, the system can produce more hydrogen from surplus electricity, which in turn requires a larger hydrogen storage capacity. As a result, the capital cost of the tank increases, leading to a moderate rise in the total investment cost.
The mechanism is therefore different from that governing the annual cost. While the annual cost is mainly influenced by OPEX, especially the electricity purchased from

the grid, the investment cost is driven by CAPEX and by the sizing of the main system components. In particular, the increase in hydrogen production associated with larger PV capacities leads to a larger storage requirement in the cost-minimization scenario, and therefore to a higher investment cost.

4.2 Hydrogen-related considerations

The hydrogen-related results are discussed in terms of the storage capacity selected by the optimization for the different installed PV capacities. Table 4.3 reports the hydrogen tank capacity obtained in each scenario and allows a direct comparison of the sizing choices made under the two extreme optimization objectives.

Table 4.3: Total Installed Capacity of the Hydrogen Tank [kg] for Different Installed Power Scenarios

	12 kW	18 kW	24 kW
Minimization of Total Cost	2.95	3.36	3.38
Maximization of Emission Reduction	117.63	116.29	108.91

Under the cost-minimization objective, the optimization tends to select the smallest hydrogen storage capacity compatible with system operation. This result is consistent with the economic structure of the problem, since the hydrogen tank has a significant impact on the total capital cost, as discussed in the previous Section 4.1. Therefore, when the objective is to minimize the total system cost, the model limits the amount of hydrogen stored and avoids oversizing the tank. For this reason, the hydrogen-storage results in the cost-minimization case can be interpreted mainly as a consequence of CAPEX reduction. In other words, the optimization does not aim to maximize hydrogen utilization, but rather to keep the storage system as small as possible while still ensuring feasible operation.

A different behavior is observed under the emission-minimization objective. In this case, the total hydrogen produced is not highest for the 12 kW scenario, but increases for the larger PV capacities. More specifically, the 12 kW case is associated with a lower total hydrogen production than the 18 kW and 24 kW cases, which

is consistent with the lower amount of PV surplus available for electrolysis. This results are shown in the Table 4.4

Table 4.4: Hydrogen-Related Results for Different Installed Power Scenarios

	Total H_2 produced [kg]	**Maximum H_2 stocked [kg]**	**Total overproduction [kWh]**
12 kW	676.59	117.63	24988
18 kW	752.71	116.29	42140
24 kW	761.59	108.91	49200

However, although the total hydrogen production is lower in the 12 kW case, the maximum hydrogen stored is higher, and this leads to a larger tank size. This apparent contradiction can be explained by the temporal distribution of the PV surplus. With 12 kW of installed PV capacity , the surplus electricity available for hydrogen production is lower overall, but it is concentrated in fewer time intervals, so the hydrogen produced must be accumulated over shorter periods and stored more intensively. As a result, the peak storage requirement is higher. By contrast, for 18 kW and especially 24 kW, the larger PV system generates more surplus electricity over the year, which leads to a higher total hydrogen production. At the same time, so the hydrogen does not accumulate in the tank with the same peak intensity observed in the 12 kW case. Consequently, the required maximum storage capacity decreases even though the total amount of hydrogen produced is higher.

These results show that hydrogen tank sizing is not determined only by the total hydrogen produced, but also by the temporal profile of surplus electricity and hydrogen generation. In the emission-minimization scenario, increasing the installed PV capacity leads to greater hydrogen production, while simultaneously reducing the maximum storage requirement due to a more distributed operating pattern.

4.3 Emission and environmental implications

The environmental performance of the system is evaluated in terms of CO_2 emission reduction for different installed PV capacities. As shown in Figure 4.3, the percentage

of avoided emissions increases as the installed PV capacity rises for both optimization objectives. This trend is expected, since a larger PV system allows a grater share of the energy demand to be covered by on-site renewable generation, thereby reducing the amount of electricity purchased from the grid.

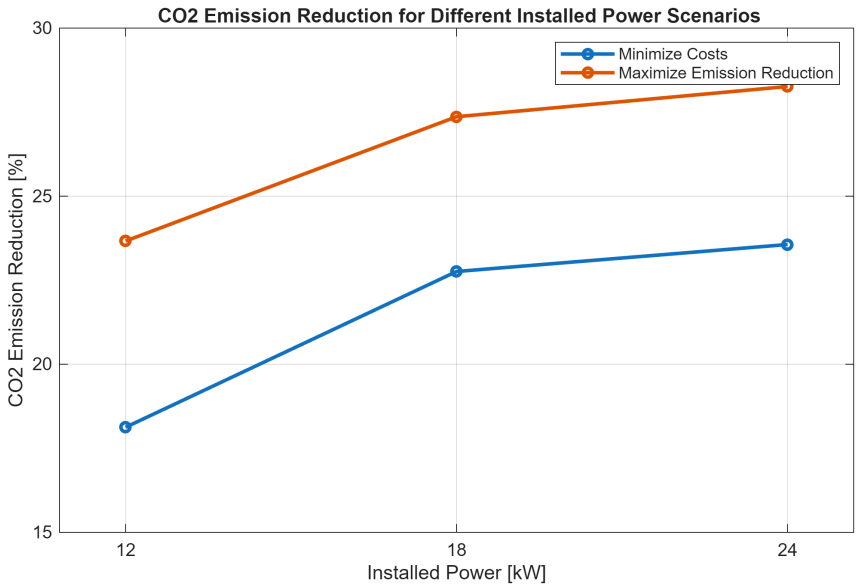

Figure 4.3: CO_2 Emission Reduction [%] for Different Installed Power Scenarios

In addition to this direct effect, a second mechanism contributes to the emission reduction. As the installed PV capacity increases, the amount of surplus electricity available for electrolysis also increases, enabling higher hydrogen production, as seen in Section 4.2. The hydrogen can then be used within the system as an energy carrier, contributing to a further reduction in the use of externally supplied energy and, consequently, in the associated CO_2 emissions. The increase in emission reduction is therefore the result of a combined effect. On the one hand, larger PV capacity directly lowers grid dependence; on the other hand, it enhances hydrogen production and use, which improves the overall capability of the system to exploit renewable energy. This explains why the percentage of CO_2 emission reduction grows with installed PV power in both optimization cases.

A comparison between the two objectives also shows that the emission-minimization strategy achieves higher environmental benefits for all PV capacities. This is consistent with the nature of the optimization objective, which prioritizes the reduction of environmental impact and therefore promotes solutions characterized by a more intensive use of renewable generation and hydrogen-based energy shifting.

4.4 Thermal considerations

The thermal results of the cogeneration system are analyzed by considering the heat exchanged during SOFC and SOEC operation, as well as the thermal energy storage capacity selected by the optimization. In all the simulated scenarios, the TES is never selected by the model, resulting in an installed storage capacity equal to 0 kWh. This outcome indicates that thermal storage does not provide an additional benefit under the investigated operating conditions. A possible explanation is that the heat produced during SOFC operation is approximately balanced by the heat absorbed during SOEC operation, so that the overall thermal exchanges within the system are nearly compensated. As a consequence, the optimization does not identify a need for dedicated thermal storage, since the thermal balance can already be managed through the intrinsic interaction between the two operating modes.
From this perspective, the system does not exhibit a significant cogenerative contribution in terms of recoverable surplus heat. In other words, the heat generated in fuel cell mode is largely neutralized by the thermal demand of the electrolysis mode, and therefore no additional TES capacity is required.
For this reason, Tables 3.5, 3.10 and 3.15 report the heat exchanged in SOFC and SOEC modes only for all the simulations. The reported values show that the thermal contributions of the two modes are of the same order of magnitude, which explains why TES is systematically excluded from the optimal configuration.

4.5 Limitations of the analysis

Despite the relevance of the obtained results, the present analysis is affected by some limitations that should be considered when interpreting the outcomes.
First, the optimization relies on a simplified representation of the system, in which component performance, investment costs and emission factor as treated according to fixed model assumptions, as described in Chapter 2. As a consequence, the results depend on the selected parameters and may vary if different techno-economic inputs are adopted.
Second, the analysis is based on a limited set of installed PV capacities and on a restricted number of optimization objectives. Although this choice was useful to highlight the main trends of the system, it does not allow a fully continuous

exploration of the design space. Therefore, some local irregularities observed in the results may be associated with the discrete nature of the investigated scenarios.
Another relevant limitation concerns the simplified treatment of system operation. Dynamic effects such as component degradation, start-up and shut-down constraints, part-load thermal behavior and control-related limitations were not explicitly investigated. In real applications, these aspects may influence both the operation strategy and the resulting component sizing.
Moreover, the environmental assessment was limited to the operational CO_2 emissions associated with energy use. A more comprehensive evaluation could include life-cycle aspects, such as embodied emissions related to PV panels, hydrogen storage and auxiliary components.

For these reasons, the results presented in this work should be interpreted as a comparative assessment within the selected modelling assumptions.

4.6 Future developments

Several future developments may improve the robustness and applicability of the present analysis. First, the modelling framework could be refined by adopting more realistic assumptions for the main components, including part-load behavior, degradation effects and start-up/shut-down constraints. These aspects may influence both the optimal sizing and the operational strategy of the system.
A further improvement would be the extension of the analysis to a wider set of design scenarios. In particular, additional PV capacities, alternative storage configurations and full sensitivity analyses on techno-economic parameters could provide a more complete exploration of the solution space. This would also help clarify whether some of the local deviations observed in the results are due to the discrete nature of the investigated cases.
The current formulation enforces a fixed dispatch hierarchy in which grid electricity purchased is treated as a last resort, regardless of electricity price conditions. A promising extension would be to relax this constraint and allow the optimizer to choose between grid purchase and hydrogen discharge based on real-time price signals. This would enable price-based arbitrage strategies - for instance, preserving stored hydrogen for high-price hours while purchasing cheap grid electricity during low-price periods - potentially improving the economic performance of the system.

Future work could also include a more detailed environmental assessment. In the present study, the analysis mainly focused on operational emissions, whereas a more comprehensive evaluation could account for life-cycle impacts associated with PV modules, hydrogen storage and auxiliary system components.

Finally, the model could be tested under more realistic operating conditions by applying the methodology to a real case study. This would make it possible to assess the practical reliability of the proposed approach and to verify whether the same trends remain valid under real operating conditions.

Chapter 5

Conclusions

This thesis investigates the optimal operation of a reversible Solid Oxide Cell (rSOC) integrated into two photovoltaic energy communities interconnected by a shared hydrogen storage system. The study was motivated by the structural mismatch between variable PV generation and local energy demand, which leads to recurring surplus electricity that, without adequate storage, would otherwise be injected back into the distribution grid. The proposed system addresses this challenge by coupling hydrogen production via Solid Oxide Electrolyzer Cell (SOEC) mode with electricity recovery via Solid Oxide Fuel Cell (SOFC) mode, along with a Thermal Energy Storage (TES) for potential cogeneration support.

A Mixed-Integer Linear Programming (MILP) optimization model was developed in Python using Pyomo and solved with Gurobi, enabling the simultaneous optimization of electricity, hydrogen and thermal energy flows over an hourly time horizon. The model was applied to a case study inspired by the real energy community "La Lleva Cominutat Energètica" in Santa Maria de Palautordera (Barcelona, Spain), considering three PV installation scenarios (12, 18 and 24 kWp total) and a bi-objective formulation that trades off total system cost against CO_2 emission reduction through a weighted-sum approach.

The results consistently show that the integration of an rSOC-based hydrogen storage system enables a meaningful reduction of grid electricity purchases and associated CO_2 emissions across all scenarios. Emission reductions range from approximately 18% under pure cost minimization with 12 kWp, to nearly 28% under emission maximization with 24 kWp installed capacity. As the installed PV capacity

increases, both the CO_2 reduction and the annual cost savings improve, thanks to the combined effect of greater on-site generation and more surplus electricity available for hydrogen production.

However, the economic assessment reveals that the system is not yet economically competitive with the reference configuration, direct grid electricity and natural gas supply, under the investigated techno-economic assumptions. Economic annual losses with respect to the reference case range between approximately 43% and 66% depending on the objective weights and installed capacity. This outcome hold even when a substantially reduced rSOC CAPEX (-60% relative to the current market baseline) is assumed, reflecting an optimistic technology learning trajectory. The primary driver of this unfavorable economics is the high capital cost of the hydrogen storage tank, which scales directly with the amount of hydrogen produced and scales significantly when emission reduction is prioritized.

Regarding the thermal pathway, the TES was never selected by the optimizer in any of the simulated cases, resulting in an installed thermal storage capacity of 0 kWh across all scenarios and all objective configurations. This result is explained by the near-balance between the heat generated during SOFC operation and the heat absorbed during SOEC operation: since the two thermal contributions are of comparable magnitude and opposite sign, the net recoverable heat available for cogeneration is negligible and no dedicated thermal storage capacity is justified by the optimization. Consequently, the thermal demand of the energy communities is almost entirely covered by natural gas through conventional boilers.

These findings collectively indicate that, under present-day cost structures, the rSOC system functions primarily as a tool for emission reduction rather than for economic optimization. The trade-off between cost and environmental performance is clearly captured by the bi-objective formulation:increasing the weight assigned to emission minimization leads to substantially larger hydrogen tank sizes and higher net present costs, but yields progressively higher CO_2 reductions. Since no single solution simultaneously minimizes cost and maximizes emission reduction, this result underlines the importance of providing policymakers and community managers with multi-objective decision support tools rather than single-objective assessments.

Future developments should address these limitations by incorporating more physically detailed component models, extending the scenario space to a wider range

of PV capacities and storage configurations and applying the methodology to a real case study with measured demand data. The current formulation also enforces a fixed dispatch hierarchy in which grid purchase is always treated as a last resort; relaxing this constraint to allow price-based arbitrage - preserving stored hydrogen for high-price hours while purchasing cheap grid electricity when prices are low - could improve the economic performance of the system. A more comprehensive life-cycle environmental assessment would also strengthen the sustainability conclusions. Additionally, as solid oxide technologies continue to mature and their costs decrease through learning-by-doing and economies of scale, repeating the analysis with updated techno-economic parameters could significantly alter the economic outlook and potentially demonstrate the viability of rSOC-based systems for residential energy communities.

In summary, this thesis demonstrates that MILP-based optimization is an effective tool for assessing multi-vector energy communities incorporating reversible solid oxide cells. The rSOC enables technically valid hydrogen-mediated energy shifting and measurable emission reductions, but its economic deployment in residential-scale communities currently requires either a substantial further reduction in component costs or a supportive policy framework - such as carbon pricing or investment incentives - to become competitive with conventional energy supply alternatives.

Bibliography

[1] Eliodoro Chiavazzo. Energy storage: Lecture slides. Course material, Politecnico di Torino, 2024.

[2] Elcogen. *Solid oxide stacks for fuel cell systems*. Elcogen. Accessed: 2026-02-25.

[3] Jens Lowitzsch, Christina E. Hoicka, and Frans J. van Tulder. Renewable energy communities under the 2019 european clean energy package – governance model for the energy clusters of the future? *Renewable and Sustainable Energy Reviews*, 122:109489, 2020.

[4] Francesco Demetrio Minuto and Andrea Lanzini. Energy-sharing mechanisms for energy community members under different asset ownership schemes and user demand profiles. *Renewable and Sustainable Energy Reviews*, 168:112859, 2022.

[5] Ricardo Moura and Miguel Centeno Brito. Prosumer aggregation policies, country experience and business models. *Energy Policy*, 132:820–830, 2019.

[6] Francisco Belmar, Patrícia Baptista, and Diana Neves. Modelling renewable energy communities: assessing the impact of different configurations, technologies and types of participants. *Energy, Sustainability and Society*, 13(1):18, 2023.

[7] Elissaios Sarmas, Evangelos Spiliotis, Vangelis Marinakis, Marco Antonio Bucarelli, Francesca Santori, and Haris Doukas. Revving up energy autonomy: A forecast-driven framework for reducing reverse power flow in microgrids. *Sustainable Energy, Grids and Networks*, 38:101376, 2024.

[8] M. Califano, M. Sorrentino, M. A. Rosen, and C. Pianese. Optimal heat and power management of a reversible solid oxide cell based microgrid for effective technoeconomic hydrogen consumption and storage. *Applied Energy*, 319:119268, 2022.

[9] National Institute of Standards and Technology (NIST). Guide for the use of the international system of units (si) — appendix b.8: Factors for units listed alphabetically. https://physics.nist.gov/Pubs/SP811/appenB8.html, n.d. Accessed: 2026-02-11.

[10] N. Rispoli, F. Vitale, F. Califano, M. Califano, P. Polverino, M. A. Rosen, and M. Sorrentino. Constrained optimal design of a reversible solid oxide cell-based multiple load renewable microgrid. *Journal of Energy Storage*, 31:101570, 2020.

[11] Paula Muñoz-Peña, Lorenzo Bruno, Aleix Señís, Marina Fajardo, Marc Cheah-Mane, Oriol Gomis-Bellmunt, and Eduardo Prieto-Araujo. Optimal design of a hydrogen system of grid-connected flexible industrial microgrids. In *Proceedings of the 23rd Wind & Solar Integration Workshop*, Helsinki, Finland, October 2024. CITCEA, Universitat Politècnica de Catalunya and Schneider Electric.

[12] Gang Xiao, Anwei Sun, Hongwei Liu, Meng Ni, and Haoran Xu. Thermal management of reversible solid oxide cells in the dynamic mode switching. *Applied Energy*, 331:120383, 2023.

[13] Paolo Marocco, Domenico Ferrero, Emanuele Martelli, Massimo Santarelli, and Andrea Lanzini. An MILP approach for the optimal design of renewable battery-hydrogen energy systems for off-grid insular communities. *Energy Conversion and Management*, 245:114564, 2021.

[14] David Bionaz, Paolo Marocco, Domenico Ferrero, Kyrre Sundseth, and Massimo Santarelli. Life cycle environmental analysis of a hydrogen-based energy storage system for remote applications. *Energy Reports*, 8:5080–5092, 2022.

[15] Paolo Marocco, Marta Gandiglio, and Massimo Santarelli. Optimal design of PV-based grid-connected hydrogen production systems. *Journal of Cleaner Production*, 434:140007, 2024.

[16] Oleg Grodzevich and Oleksandr Romanko. Normalization and other topics in multi-objective optimization. In *Proceedings of the Fields-MITACS Industrial Problems Workshop*, pages 89–101, 2006. Report prepared for Algorithmics Inc.

[17] Sebastian Miehling, Andreas Hanel, Jerry Lambert, Sebastian Fendt, and Hartmut Spliethoff. Energy system optimisation using (mixed integer) linear programming: Description of a framework for 'optimal technology utilisation in multi-sectoral applications' (optumus). *arXiv preprint arXiv:2308.01882*, August 2023. Chair of Energy Systems.

[18] Michael L. Bynum, Gabriel A. Hackebeil, William E. Hart, Carl D. Laird, Bethany L. Nicholson, John D. Siirola, Jean-Paul Watson, and David L. Woodruff. *Pyomo–optimization modeling in python*, volume 67. Springer Science & Business Media, third edition, 2021.

[19] Gurobi Optimization, LLC. Gurobi Optimizer Reference Manual, 2024.

[20] Som Comunitats. Comunitats energètiques per ajuntaments (administració pública). https://somcomunitats.coop/administracio/. Accessed: 2025-10-15.

[21] La Lleva. La lleva (comunitat energètica del baix montseny sccl) – website. https://www.lalleva.cat/. Accessed: 2025-10-15.

[22] Google LLC. Google earth (distance measurement tool). https://earth.google.com/. Distance measured on 2025-10-15.

[23] Dataset (csv download), view hx6q-ykhb. https://analisi.transparenciacatalunya.cat/api/views/hx6q-ykhb/rows.csv?accessType=DOWNLOAD. Accessed: 2025-10-22.

[24] Acis Energía. ¿qué potencia de luz contratar según tu tipo de hogar? https://acisenergia.com/blog/sabes-que-potencia-contratar/. Accessed: 2025-10-22.

[25] Ministerio de Ciencia y Tecnología (España). Guía-bt-10: Guía técnica de aplicación. instalaciones de enlace. previsión de cargas para suministros en baja tensión. Technical Report Revisión 1, Ministerio de Ciencia y Tecnología, September 2003. Accessed: 2026-01-19.

[26] Institut Català d'Energia (ICAEN). Balanç energètic (web page). https://icaen.gencat.cat/es/energia/estadistiques/resultats/anuals/balanc_energetic/. Accessed: 2025-11-11.

[27] ENEA. Conversione, fattori di. https://www.efficienzaenergetica.enea.it/glossario-efficienza-energetica/lettera-c/conversione-fattori-di.html. Accessed: 2025-11-11.

[28] Ricardo García San José and Arcadio García Lastra. *Rendimiento medio estacional en instalaciones de calefacción. Parte teórica. Guías IDAE 014*. Instituto para la Diversificación y Ahorro de la Energía (IDAE), Madrid, Spain, October 2017. Guía técnica. Redactada por ATECYR para IDAE.

[29] Servei Meteorològic de Catalunya (Meteocat). Sèrie climàtica de barcelona des de 1780 (temperatura mitjana mensual). https://www.meteo.cat/wpweb/climatologia/dades-i-productes-climatics/serie-climatica-de-barcelona-des-de-1780/. Accessed: 2026-02-06.

[30] Servei Meteorològic de Catalunya (Meteocat). Dades d'estacions: graus-dia de calefacció i de refrigeració (gdc/gdr). https://www.meteo.cat/wpweb/climatologia/dades-i-productes-climatics/graus-dia-de-calefaccio-i-de-refrigeracio/dades-estacions-graus-dia-de-calefaccio-i-de-refrigeracio/. Accessed: 2026-02-06.

[31] Ministerio de Vivienda y Agenda Urbana. Documento Básico HE: Ahorro de energía (CTE), June 2022. Texto consolidado, 14 junio 2022.

[32] FEGECA. Guía práctica sobre instalaciones individuales de calefacción y agua caliente sanitaria (ACS) en edificios de viviendas, February 2011. Depósito Legal: M-9197-2011.

[33] Timothy Doak Steele. A simple-harmonic model for depicting the annual cycle of seasonal temperatures of streams. Open-File Report 78-155, U.S. Geological Survey, Lakewood, Colorado, March 1978. Paper presented at the Symposium and Workshops on the Application of Mathematical Models in Hydrology and Water Resources Systems, Bratislava, Czechoslovakia, Sept. 8–13, 1975.

[34] Servei Meteorològic de Catalunya (Meteocat). Sèries climàtiques des de 1950. https://www.meteo.cat/wpweb/climatologia/dades-i-productes-climatics/series-climatiques-des-de-1950/, 2026. Accessed: 2026-02-10.

[35] Institut d'Estadística de Catalunya (Idescat). Edificis destinats principalment a habitatge. per estat de conservació (catalunya, 2011). https://www.idescat.cat/pub/?id=cense&n=6065. Accessed: 2026-02-10. Source: Idescat, based on INE Building Census (Cens d'edificis de l'INE).

[36] Elcogen AS. *Solid oxide stacks for electrolyser systems*. Elcogen, Tallinn, Estonia, 2024. Technical specifications for elcoStack E3000, E1000, and E350 models.

[37] Marco Bogar. Water electrolysis and electrolyser technologies - part 3. Lecture notes for the course "Hydrogen and Fuel Cells", 2023. A.A. 2023-2024.

[38] Franco Bagatti, Elisabetta Corradi, Alessandro Desco, and Claudia Ropa. *Chimica*. Zanichelli Editore S.p.A., Bologna, 2 edition, 2017. Capitolo 10: Trasformazioni della materia: energia e ambiente.

[39] LibreTexts. 19.13: The temperature dependence of δh. Chemistry LibreTexts, 2021.

[40] M. Chen and X. Sun. Thermoneutral operation of solid oxide electrolysis cells. https://ecs.confex.com/ecs/sofc2017/webprogram/Paper101149.html. ECS Meeting Abstracts / SOFC-XV (2017). Accessed: 2026-02-25.

[41] Subhash C. Singhal. Solid oxide fuel cells for power generation. *WIREs Energy and Environment*, 3:179–194, 2014.

[42] Gruppo Sapio. *O2 OSSIGENO - Scheda Tecnica*. Sapio Produzione Idrogeno Ossigeno S.r.l., 2024. Proprietà fisiche e specifiche tecniche del gas ossigeno.

[43] Gruppo Sapio. *H2 IDROGENO - Scheda Tecnica*. Sapio Produzione Idrogeno Ossigeno S.r.l., 2024. Proprietà fisiche e specifiche tecniche del gas idrogeno.

[44] Peter J. Linstrom and William G. Mallard. Nist chemistry webbook, NIST standard reference database number 69. https://webbook.nist.gov/cgi/cbook.cgi?ID=C7732185, 2001. National Institute of Standards and Technology.

[45] Massimo Santarelli. Polygeneration and advanced energy systems: Lecture slides. Course material, Politecnico di Torino, 2024.

[46] Nicholas Klymyshyn, Kriston Brooks, and Nathan Barrett. Methods for estimating hydrogen fuel tank characteristics. *Journal of Pressure Vessel Technology*, 2024.

[47] Pegah Mottaghizadeh, Srikanth Santhanam, Marc P. Heddrich, K. Andreas Friedrich, and Fabio Rinaldi. Process modeling of a reversible solid oxide cell r-soc energy storage system utilizing commercially available soc reactor. *Energy Conversion and Management*, 2017.

[48] Andrew Russell Solano, Austin Clark, Kent P. Detrick, Matthew J. Memmott, and Stella D. Nickerson. Characterization of the molten salt fmgnak through ab initio molecular dynamics and experimental density measurements. *Journal of Nuclear Materials*, 2021. Accessed: 2025-11-21.

[49] Austin David Clark. *Structural Characteristics and Thermophysical Properties of Molten Salts from Ab Initio Molecular Dynamics Simulations*. Ph.d. dissertation, Brigham Young University, 2021. Accessed: 2025-11-21.

[50] Yang Wang, Xiang Li, Huiqin Yin, and Zhongfeng Tang. Design optimization and thermophysical characteristics of naf–kcl reciprocal salts by theoretical predictions and experimental measurements for the high latent heat storage. *Thermal Science and Engineering Progress*, 37:101591, 2023.

[51] STEX24. Power and capacity: Understanding the difference, 2024. Accessed: 2025-02-17.

[52] J. Donoso, M. Behar, and A. Miranda. National survey report of pv power applications in spain 2023. Technical report, IEA Photovoltaic Power Systems Programme (IEA-PVPS), Task 1, December 2023.

[53] Central Electricity Regulatory Commission (CERC). Explanatory memorandum for cerc draft (terms and conditions for tariff determination from renewable energy sources) (fifth amendment) regulations, 2016. Technical report, Central Electricity Regulatory Commission (CERC), 2016.

[54] Christof Bernsteiner, Johanna Ganglbauer, Evelyn Hummer, and Robert Pratter. Analysis of rsoc systems to support the energy supply of modern positive energy districts. In *REAL CORP 2025 Proceedings*, April 2025.

[55] The impact of pv module reliability on plant lifetimes exceeding 25 years. https://www.energy.gov/eere/solar/articles/impact-pv-module-reliability-plant-lifetimes-exceeding-25-years.

[56] Frost & Sullivan. Elcogen as: Enabling technology leader. Technical report, Frost & Sullivan, 2025.

[57] Martin Andersson and Jan Froitzheim. Technology review – solid oxide cells 2019. Technical Report 2019:601, Energiforsk AB, August 2019.

[58] V. Cigolotti and M. Genovese. Stationary fuel cell applications: Current and future technologies – costs, performances, and potential. Technical report, ENEA (Italian National Agency for New Technologies, Energy and Sustainable Economic Development) and University of Calabria, 2021.

[59] Joshua Mermelstein and Oliver Posdziech. Development and demonstration of a novel reversible sofc system for utility and micro grid energy storage. *Fuel Cells*, 17(4):562–570, 2017.

[60] European Central Bank. Ecb data portal: Spot us dollar/euro exchange rate (annual average), series exr.a.usd.eur.sp00.a. https://data.ecb.europa.eu/data/datasets/EXR/EXR.A.USD.EUR.SP00.A.

[61] Dieter Braun GmbH. Copper price (information center). https://kabelkonfektion.com/en/information-center/copper-price/.

[62] Red Eléctrica de España (REE). Esios: Precio mercado spot diario españa (indicator 600). https://www.esios.ree.es/es/analisis/600.

[63] MIBGAS. Mibgas: Gas daily price index and volumes (daily price index). https://www.mibgas.es/en/market-results/gas-daily-price-index-and-volumes.

[64] UNEF. El autoconsumo fotovoltaico en españa alcanza los 9,3 gw instalados, January 2026.

[65] Hans van 't Noordende, Frans van Berkel, and Maciej Stodolny. Next level solid oxide electrolysis: Upscaling potential and techno-economical evaluation for 3 industrial use cases, 2023.

[66] Christof Bernsteiner, Johanna Ganglbauer, Evelyn Hummer, and Robert Pratter. Analysis of rsoc systems to support the energy supply of modern positive energy districts. In *REAL CORP 2025 Proceedings*, 2025.

[67] International Renewable Energy Agency. Green hydrogen cost reduction: Scaling up electrolysers to meet the 1.5°c climate goal, 2020.

[68] U.S. Department of Energy. Clean hydrogen production cost scenarios with pem electrolyzer technology. Technical Report Program Record 24005, DOE Hydrogen and Fuel Cell Technologies Office, 2024.

Appendix A

H2.py

Here, the script that describes the most significant part of the optimization is attached. First, the time steps in which a surplus or deficit occurs are identified. For surplus, this means the amount of electricity produced by the PV that exceeds the electric demand, while for deficit, it means the amount of electricity demand that is not satisfied by the PV. These time steps are coupled with the operation of the reversible Solid Oxide Cell (rSOC) in SOEC or SOFC mode: in surplus conditions the rSOC operates in SOEC mode, while in deficit conditions it operates in SOFC mode. Moreover, the time steps in which a switch occurs are detected. Then, the amount of hydrogen produced is evaluated based on the specific energy consumption. Also, the electricity produced per kilogram of hydrogen is evaluated, together with the amount of hydrogen consumed and stored. In this script, the thermal part of the system is also evaluated: the thermal energy released and required by the rSOC system, the thermal balance between the thermal demand and the thermal energy bought from the gas distributor, and the balances of the Thermal Energy Storage system.

Listing A.1: H2.py

```
1
2 import pyomo.environ as pyo
3 import pre_processing
4
5 def H2_block(model, l_t, AllInputs):
6     #model.t = pyo.Set(initialize=l_t) (defined before, it is
          the time of one year, in hours)
7     model.i_bus = pyo.Set(initialize=AllInputs.Buses.id_list)
8
```

```
9     model.PV_fore = pyo.Reference(model.PV_prod)
10
11    model.demand = pyo.Param(model.t, initialize=pre_processing
          .demand_tot.iloc[:, 0].to_dict(), within=pyo.
          NonNegativeReals) #kW
12    model.spec_en_consump = pyo.Param(initialize=AllInputs.SOEC
          .sp_energycons, within=pyo.NonNegativeReals) #kWh/kg
13    model.LHV_H2 = pyo.Param(initialize=AllInputs.SOFC.LHV_H2,
          within=pyo.NonNegativeReals) #MJ/kg
14    model.SOFC_eff = pyo.Param(initialize=AllInputs.SOFC.
          gross_eff, within=pyo.NonNegativeReals) #%
15
16    model.SOEC_enthalpy = pyo.Param(initialize=AllInputs.SOEC.
          enthalpy, within=pyo.Reals) #kJ/mol deltah<0
17    model.SOFC_enthalpy = pyo.Param(initialize=AllInputs.SOFC.
          enthalpy, within=pyo.Reals) #kJ/mol deltah>0
18    model.MW_H2 = pyo.Param(initialize=AllInputs.SOFC.MW_H2,
          within=pyo.NonNegativeReals) #g/mol
19    model.MW_O2 = pyo.Param(initialize=AllInputs.SOFC.MW_O2,
          within=pyo.NonNegativeReals) #g/mol
20    model.MW_H2O = pyo.Param(initialize=AllInputs.SOFC.MW_H2O,
          within=pyo.NonNegativeReals) #g/mol
21    model.max_cap_H2 = pyo.Param(initialize=AllInputs.Tank.
          maxcapacity, within=pyo.NonNegativeReals) #kg
22
23    model.RTE_TES = pyo.Param(initialize=AllInputs.TES.RTE_TES,
           within=pyo.NonNegativeReals) #pu
24    model.th_demand = pyo.Param(model.t, initialize=AllInputs.
          Thermal.Pt, within=pyo.Reals) #kWh
25    model.max_cap_TES = pyo.Param(initialize=AllInputs.TES.
          max_cap, within=pyo.NonNegativeReals)
26    model.initial_TES = pyo.Param(initialize=AllInputs.TES.
          init_charge, within=pyo.Reals)
27
28    model.SOEC_on = pyo.Var(model.t, within=pyo.
          NonNegativeReals, bounds=(0, 1)) # to define the mode
          operation
29    model.SOFC_on = pyo.Var(model.t, within=pyo.
          NonNegativeReals, bounds=(0, 1))
30    model.is_surplus = pyo.Var(model.t, within=pyo.
          NonNegativeReals, bounds=(0, 1)) # 1 if PV > demand
31    model.is_switching = pyo.Var(model.t, within=pyo.
          NonNegativeReals, bounds=(0, 1))  # 1 if it is switching
```

```
32
33      model.overproduction = pyo.Var(model.t, within=pyo.
            NonNegativeReals)
34      model.H2_produced = pyo.Var(model.t, within=pyo.
            NonNegativeReals) #kg
35      elec_per_kg = (AllInputs.SOFC.gross_eff / 100) * (AllInputs
            .SOFC.LHV_H2 / 3.6) #I evaluate the electricity produced
             [kWh] with a kg of H2. It is done multiplying the SOFC
            efficiency with the lower heating value of H2
36      model.electricity_for_1kg = pyo.Param(initialize=
            elec_per_kg, within=pyo.NonNegativeReals) #kWh per 1 kg
            of H2 (kWh/kg)
37
38      model.electricity_deficit = pyo.Var(model.t, within=pyo.
            NonNegativeReals) #kWh , amount that the PV can't
            satisfy
39      model.H2_consumed = pyo.Var(model.t, within=pyo.
            NonNegativeReals)
40      model.electricity_produced = pyo.Var(model.t,within=pyo.
            NonNegativeReals) #kWh
41      model.H2_stocked = pyo.Var(model.t, within=pyo.
            NonNegativeReals)
42      model.H2_to_tank = pyo.Var(model.t, within=pyo.
            NonNegativeReals)
43      model.H2_from_tank = pyo.Var(model.t, within=pyo.
            NonNegativeReals)
44
45      model.el_to_buy = pyo.Var(model.t, within=pyo.
            NonNegativeReals)  # kWh electricity purchased from the
            grid
46
47      model.overprod_times_not_switching = pyo.Var(model.t,
            within=pyo.NonNegativeReals)  # overproduction    (1 -
            0.5*is_switching)
48
49      model.th_energy_realised = pyo.Var(model.t, within=pyo.
            NegativeReals) #kWh; energy realised from SOFC mode
50      model.th_energy_requested = pyo.Var(model.t, within=pyo.
            NonNegativeReals) #kWh; energy assorbed by SOEC mode
51      model.P_th_rSOC = pyo.Var(model.t, within=pyo.Reals) #kW;
            thermal power of rSOC
```

```
52      model.P_boilers = pyo.Var(model.t, within=pyo.
            NonNegativeReals)  # kW - thermal power from the gas
            distributor
53      model.P_th_TES = pyo.Var(model.t, within=pyo.Reals)  # kW -
             pthermal power entering (>0) or exiting (<0) from the
            TES
54      model.Q_in = pyo.Var(model.t, within=pyo.NonNegativeReals)
             # kWh - energy entering in the TES
55      model.Q_out = pyo.Var(model.t, within=pyo.NonNegativeReals)
              # kWh - energy exiting from the TES
56      model.TES_stored = pyo.Var(model.t, within=pyo.
            NonNegativeReals)  # kWh - energia accumulata nel TES
57      model.is_TES_charging = pyo.Var(model.t, within=pyo.
            NonNegativeReals, bounds=(0, 1))  # 1 if TES is charging
            , 0 if is discharging
58
59      max_PV = pre_processing.PV_tot.iloc[:, 0].max()  # kW
60      max_demand = pre_processing.demand_tot.iloc[:, 0].max()  #
            kW
61
62      def Detect_surplus(m, t):
63          M = max_PV + max_demand
64          return m.PV_fore[t] - m.demand[t] <= M * m.is_surplus[t
                ]
65      model.Detect_surplus = pyo.Constraint(model.t, rule=
            Detect_surplus)
66
67      def Detect_deficit(m, t):
68          M = max_PV + max_demand
69          return m.demand[t] - m.PV_fore[t] <= M * (1 - m.
                is_surplus[t])
70      model.Detect_deficit = pyo.Constraint(model.t, rule=
            Detect_deficit)
71
72      def Mode_SOEC(m, t):
73          return m.SOEC_on[t] == m.is_surplus[t]
74      model.Mode_SOEC = pyo.Constraint(model.t, rule=Mode_SOEC)
75
76      def Mode_SOFC(m, t):
77          return m.SOFC_on[t] == 1 - m.is_surplus[t]
78      model.Mode_SOFC = pyo.Constraint(model.t, rule=Mode_SOFC)
79
80      def Detect_switch_1(m, t):
```

```
81          if t == m.t.first():
82              return pyo.Constraint.Skip
83          return m.is_switching[t] >= m.SOEC_on[t] - m.SOEC_on[t
                - 1]
84      model.Detect_switch_1 = pyo.Constraint(model.t, rule=
            Detect_switch_1)
85
86      def Detect_switch_2(m, t):
87          if t == m.t.first():
88              return pyo.Constraint.Skip
89          return m.is_switching[t] >= m.SOEC_on[t - 1] - m.
                SOEC_on[t]
90      model.Detect_switch_2 = pyo.Constraint(model.t, rule=
            Detect_switch_2)
91
92      def Calculate_overproduction(m,t):
93          return m.overproduction[t] >= m.PV_fore[t] - m.demand[t
                ]
94      model.Calculate_overproduction = pyo.Constraint(model.t,
            rule=Calculate_overproduction)
95
96      def Force_overproduction_zero_when_deficit(m, t):
97          M = 20
98          return m.overproduction[t] <= M * m.is_surplus[t]
99      model.Force_overprod_zero_deficit = pyo.Constraint(model.t,
             rule=Force_overproduction_zero_when_deficit)
100
101     def Lin_overprod_upper(m, t):
102         return m.overprod_times_not_switching[t] <= m.
                overproduction[t]
103     model.Lin_overprod_upper = pyo.Constraint(model.t, rule=
            Lin_overprod_upper)
104
105     def Lin_overprod_with_switch(m, t):
106         M = max_PV
107         return m.overprod_times_not_switching[t] >= m.
                overproduction[t] - 0.5 * M * m.is_switching[t]
108     model.Lin_overprod_switch = pyo.Constraint(model.t, rule=
            Lin_overprod_with_switch)
109
110     def Calculate_H2_produced_linear(m, t):
111         return m.H2_produced[t] <= m.
                overprod_times_not_switching[t] / m.spec_en_consump
```

```
112     model.Calculate_H2_produced_linear = pyo.Constraint(model.t
            , rule=Calculate_H2_produced_linear)
113 
114     def H2_produced_zero_when_SOEC_off(m, t):
115         max_H2_from_overproduction = m.overproduction[t] / m.
                spec_en_consump
116         return m.H2_produced[t] <= max_H2_from_overproduction *
                m.SOEC_on[t]
117     model.H2_produced_zero_when_SOEC_off = pyo.Constraint(model
            .t, rule=H2_produced_zero_when_SOEC_off)
118 
119     def Def_deficit_upper(m, t):
120         M = max_PV + max_demand
121         return m.electricity_deficit[t] <= (m.demand[t] - m.
                PV_fore[t]) + M * m.is_surplus[t]
122     model.Def_deficit_upper = pyo.Constraint(model.t, rule=
            Def_deficit_upper)
123 
124     def Def_deficit_lower(m, t):
125         M = max_PV + max_demand
126         return m.electricity_deficit[t] >= (m.demand[t] - m.
                PV_fore[t]) - M * m.is_surplus[t]
127     model.Def_deficit_lower = pyo.Constraint(model.t, rule=
            Def_deficit_lower)
128 
129     def Def_deficit_zero_when_surplus(m, t):
130         M = max_PV + max_demand
131         return m.electricity_deficit[t] <= M * (1 - m.
                is_surplus[t])
132     model.Def_deficit_zero_when_surplus = pyo.Constraint(model.
            t, rule=Def_deficit_zero_when_surplus)
133 
134     def Limit_H2_consumed_by_needed(m, t):
135         return m.H2_consumed[t] <= m.electricity_deficit[t] / m
                .electricity_for_1kg
136     model.Limit_H2_consumed_by_needed = pyo.Constraint(model.t,
            rule=Limit_H2_consumed_by_needed)
137 
138     def Limit_H2_consumed_by_available(m, t):
139         if t == m.t.first():
140             return m.H2_consumed[t] <= m.H2_produced[t]
141         else:
```

```
142             return m.H2_consumed[t] <= m.H2_stocked[t - 1] + m.
                    H2_produced[t]
143     model.Limit_H2_consumed_by_available = pyo.Constraint(model
            .t, rule=Limit_H2_consumed_by_available)
144
145     def Force_H2_consumed_SOFC_binary(m, t):
146         M_H2 = max_PV / pyo.value(m.spec_en_consump) * 1.5
147         return m.H2_consumed[t] <= M_H2 * m.SOFC_on[t]
148     model.Force_H2_consumed_SOFC = pyo.Constraint(model.t, rule
            =Force_H2_consumed_SOFC_binary)
149
150     def Penalize_H2_consumed_during_switch(m, t):
151         M_H2 = max_PV / pyo.value(m.spec_en_consump) * 1.5
152         return m.H2_consumed[t] <= M_H2 * (1 - 0.5 * m.
                is_switching[t])
153     model.Penalize_H2_switch = pyo.Constraint(model.t, rule=
            Penalize_H2_consumed_during_switch)
154
155     def NonNegative_stock(m, t):
156         return m.H2_stocked[t] >= 0
157     model.NonNegative_stock = pyo.Constraint(model.t, rule=
            NonNegative_stock)
158
159     def Limit_H2_stock_capacity(m, t):
160         return m.H2_stocked[t] <= m.max_cap_H2
161     model.Limit_H2_stock_cap = pyo.Constraint(model.t, rule=
            Limit_H2_stock_capacity)
162
163     def Calculate_electricity_produced(m,t):
164         return m.electricity_produced[t] == m.H2_consumed[t] *
                m.electricity_for_1kg
165     model.Calculate_electricity_produced = pyo.Constraint(model
            .t, rule=Calculate_electricity_produced)
166
167     def Satisfy_deficit(m, t):
168         return m.electricity_deficit[t] == m.
                electricity_produced[t] + m.el_to_buy[t]
169     model.Satisfy_deficit = pyo.Constraint(model.t, rule=
            Satisfy_deficit)
170
171     def Calculate_th_en_requested_simple(m, t):
172         base_energy_per_kg = (1000 / m.MW_H2) * abs(m.
                SOEC_enthalpy) / 3600
```

```
173         return m.th_energy_requested[t] == m.H2_produced[t] *
                base_energy_per_kg
174     model.Calculate_th_en_requested = pyo.Constraint(model.t,
            rule=Calculate_th_en_requested_simple)
175
176     def Calculate_th_en_realised_simple(m, t):
177         base_energy_per_kg = (1000 / m.MW_H2) * m.SOFC_enthalpy
                / 3600
178         return m.th_energy_realised[t] == m.H2_consumed[t] *
                base_energy_per_kg
179     model.Calculate_th_en_realised = pyo.Constraint(model.t,
            rule=Calculate_th_en_realised_simple)
180
181     def Link_thermal_to_H2_consumption(m, t):
182         M = pyo.value(model.max_cap_TES) * 1.2
183         return m.P_th_rSOC[t] <= M * m.SOFC_on[t]
184     model.Link_thermal_to_H2_consumption = pyo.Constraint(model
            .t, rule=Link_thermal_to_H2_consumption)
185
186     def Force_th_realised_zero_when_no_H2(m, t):
187         M = pyo.value(model.max_cap_TES) * 1.2
188         return m.th_energy_realised[t] >= -M * m.SOFC_on[t]
189     model.Force_th_realised_zero = pyo.Constraint(model.t, rule
            =Force_th_realised_zero_when_no_H2)
190
191     def H2_tank_balance(m, t):
192         if t == m.t.first():
193             return m.H2_stocked[t] == m.H2_to_tank[t]
194         else:
195             return m.H2_stocked[t] == m.H2_stocked[t - 1] + m.
                    H2_to_tank[t] - m.H2_from_tank[t]
196     model.H2_tank_balance = pyo.Constraint(model.t, rule=
            H2_tank_balance)
197
198     def Link_production_to_tank(m, t):
199         return m.H2_produced[t] == m.H2_to_tank[t]
200     model.Link_production_to_tank = pyo.Constraint(model.t,
            rule=Link_production_to_tank)
201
202     def Link_consumption_from_tank(m, t):
203         return m.H2_consumed[t] == m.H2_from_tank[t]
204     model.Link_consumption_from_tank = pyo.Constraint(model.t,
            rule=Link_consumption_from_tank)
```

```
205
206     def Define_P_th_rSOC(m, t):
207         return m.P_th_rSOC[t] == -m.th_energy_realised[t] - m.
                th_energy_requested[t]
208     model.Define_P_th_rSOC = pyo.Constraint(model.t, rule=
            Define_P_th_rSOC)
209
210     def Thermal_demand_coverage(m, t):
211         sqrt_RTE = pyo.value(pyo.sqrt(m.RTE_TES))
212         return (m.P_boilers[t] + m.P_th_rSOC[t] + m.Q_out[t] *
                sqrt_RTE - m.Q_in[t] * sqrt_RTE == m.th_demand[t])
213     model.Thermal_demand_coverage = pyo.Constraint(model.t,
            rule=Thermal_demand_coverage)
214
215     def Detect_TES_charging(m, t):
216         M = pyo.value(m.max_cap_TES) * 1.2
217         return m.P_th_TES[t] <= M * m.is_TES_charging[t]
218     model.Detect_TES_charging = pyo.Constraint(model.t, rule=
            Detect_TES_charging)
219
220     def Detect_TES_discharging(m, t):
221         M = pyo.value(m.max_cap_TES) * 1.2
222         epsilon = 0.001
223         return -m.P_th_TES[t] <= M * (1 - m.is_TES_charging[t])
                + epsilon
224     model.Detect_TES_discharging = pyo.Constraint(model.t, rule
            =Detect_TES_discharging)
225
226     def Force_initial_TES_consistency(m, t):
227         if t == m.t.first():
228             if pyo.value(m.initial_TES) < 0.01:
229                 M_small = pyo.value(m.max_cap_TES)
230                 return m.Q_in[t] <= M_small * m.is_TES_charging
                        [t]
231             else:
232                 return pyo.Constraint.Skip
233         else:
234             return pyo.Constraint.Skip
235     model.Force_initial_TES_consistency = pyo.Constraint(model.
            t, rule=Force_initial_TES_consistency)
236
237     def Define_Q_in_charging_upper(m, t):
238         sqrt_RTE = pyo.value(pyo.sqrt(m.RTE_TES))
```

```
239         return m.Q_in[t] <= m.P_th_TES[t] * sqrt_RTE
240     model.Q_in_upper = pyo.Constraint(model.t, rule=
            Define_Q_in_charging_upper)
241
242     def Define_Q_in_charging_lower(m, t):
243         sqrt_RTE = pyo.value(pyo.sqrt(m.RTE_TES))
244         M = pyo.value(m.max_cap_TES) * 2
245         return m.Q_in[t] >= m.P_th_TES[t] * sqrt_RTE - M * (1 -
                m.is_TES_charging[t])
246     model.Q_in_lower = pyo.Constraint(model.t, rule=
            Define_Q_in_charging_lower)
247
248     def Force_Q_in_zero_discharging(m, t):
249         M = pyo.value(m.max_cap_TES) * 2
250         return m.Q_in[t] <= M * m.is_TES_charging[t]
251     model.Q_in_zero_discharge = pyo.Constraint(model.t, rule=
            Force_Q_in_zero_discharging)
252
253     def Define_Q_out_discharging_upper(m, t):
254         inv_sqrt_RTE = pyo.value(1 / pyo.sqrt(m.RTE_TES))
255         return m.Q_out[t] <= -m.P_th_TES[t] * inv_sqrt_RTE
256     model.Q_out_upper = pyo.Constraint(model.t, rule=
            Define_Q_out_discharging_upper)
257
258     def Define_Q_out_discharging_lower(m, t):
259         inv_sqrt_RTE = pyo.value(1 / pyo.sqrt(m.RTE_TES))
260         M = pyo.value(m.max_cap_TES) * 2
261         return m.Q_out[t] >= -m.P_th_TES[t] * inv_sqrt_RTE - M
                * m.is_TES_charging[t]
262     model.Q_out_lower = pyo.Constraint(model.t, rule=
            Define_Q_out_discharging_lower)
263
264     def Force_Q_out_zero_charging(m, t):
265         M = pyo.value(m.max_cap_TES) * 2
266         return m.Q_out[t] <= M * (1 - m.is_TES_charging[t])
267     model.Q_out_zero_charge = pyo.Constraint(model.t, rule=
            Force_Q_out_zero_charging)
268
269     def Limit_TES_discharge_by_energy_simple(m, t):
270         if t == m.t.first():
271             available = m.initial_TES
272         else:
273             available = m.TES_stored[t - 1]
```

```
274         return m.Q_out[t] <= available
275     model.Limit_TES_discharge_simple = pyo.Constraint(model.t,
            rule=Limit_TES_discharge_by_energy_simple)
276
277     def TES_energy_balance(m, t):
278         if t == m.t.first():
279             return m.TES_stored[t] == m.initial_TES + m.Q_in[t]
                    - m.Q_out[t]
280         else:
281             return m.TES_stored[t] == m.TES_stored[t - 1] + m.
                    Q_in[t] - m.Q_out[t]
282     model.TES_energy_balance = pyo.Constraint(model.t, rule=
            TES_energy_balance)
283
284     def TES_capacity_limit(m, t):
285         return m.TES_stored[t] <= m.max_cap_TES
286     model.TES_capacity_limit = pyo.Constraint(model.t, rule=
            TES_capacity_limit)
287
288     def TES_non_negative(m, t):
289         return m.TES_stored[t] >= 0
290     model.TES_non_negative = pyo.Constraint(model.t, rule=
            TES_non_negative)
291
292     def Limit_P_th_TES_by_available_energy(m, t):
293         if t == m.t.first():
294             available = m.initial_TES
295         else:
296             available = m.TES_stored[t - 1]
297         inv_sqrt_RTE = pyo.value(1 / pyo.sqrt(m.RTE_TES))
298         return -m.P_th_TES[t] <= available * inv_sqrt_RTE
299     model.Limit_P_th_TES_by_available = pyo.Constraint(model.t,
            rule=Limit_P_th_TES_by_available_energy)
300
301     def Limit_P_th_TES_charging_rate(m, t):
302         if t == m.t.first():
303             stored_prev = m.initial_TES
304         else:
305             stored_prev = m.TES_stored[t - 1]
306         available_space = m.max_cap_TES - stored_prev
307         sqrt_RTE = pyo.value(pyo.sqrt(m.RTE_TES))
308         return m.P_th_TES[t] <= available_space / sqrt_RTE
```

```
309     model.Limit_P_th_TES_charging = pyo.Constraint(model.t,
            rule=Limit_P_th_TES_charging_rate)
```

Appendix B

Results of the optimizations

Table B.1: Values common for 12 kWp installation

Parameter	**Unit**	**Value**
Max PV forecast	kW	10.35
Total PV overproduction	kWh	25516.97
Timestep with surplus PV production	–	1276

Table B.2: Main results for the 12 kWp, total cost minimization.

Parameter	**Unit**	**Value**
General		
Annual electricity demand	kWh	54596.72
Net Present Cost (NPC)	€	155781.3
Initial investment	€	47018.37
Payback time	years	N/A
Cumulative operating loss	€	63488.93
Total loss	€	110507.3
Maximum H_2 produced	kg	0.6061
Total H_2 produced	kg	518.2125
OPEX breakdown		

Continued on next page

Continued from previous page

Parameter	Unit	Value
OPEX	€	3232.67
PV	€	96
rSOC	€	3107.28
Tank H_2	€	29.22
TES	€	0
Cables	€	0.17
CAPEX breakdown		
CAPEX	€	28833.04
rSOC	€	25894
Tank H_2	€	2921.72
TES	€	0
Cables	€	17.32
Replacement		
PV	€	850.47
rSOC	€	16837.79
Tank H_2	€	495.52
TES	€	0
Cables	€	1.53
Sizing		
Maximum H_2 stored	kg	2.94627
H_2 tank capacity installed	kg	2.94627
Economic performance comparison		
Reference annual energy cost	€	4621.97
Annual cost with the proposed system	€	6738.27
Annual cost difference	€	-2116.3
Relative cost increase	%	45.79
CO_2 emissions without the system		
Electricity from the grid	kg CO_2/year	9056.41
Gas consumed	kg CO_2/year	7912.72
Total	kg CO_2/year	16969.13

Continued on next page

Continued from previous page

Parameter	Unit	Value
CO_2 emissions with the system		
Electricity from the grid	kg CO_2/year	5989.49
Gas consumed	kg CO_2/year	7903.62
Total	kg CO_2/year	13893.11
Emission reduction	kg CO_2/year	3076.02
Emission reduction	%	18.13
Electricity purchased from grid		
Total electricity purchased	kWh	25165.94
Cost of electricity purchased	€	1798.25
Average electricity purchased per time step	kWh	2.86498
Time step with grid purchase	–	6291
Thermal balance		
Heat produced by boilers	kWh	43426.49
Cost of gas purchased	€	1707.35
Heat produced by rSOC (SOFC)	kWh	17761.95
Heat absorbed by rSOC (SOEC)	kWh	-17711.96
Heat produced by TES (discharge)	kWh	0
Heat absorbed by TES (charge)	kWh	0
TES charging energy, Q_{in}	kWh	0
TES discharging energy, Q_{out}	kWh	0
Variation in TES stored energy	kWh	0
Maximum power boilers	kW	31.45
Time step with gas purchase	–	5112

Table B.3: Main results for the 12 kWp, under different objective-weight configurations.

Parameter	Unit	0.5/0.5	0.4/0.6	0.3/0.7	0.2/0.8	0.1/0.9
General results						
Net present cost (NPC)	€	157447.23	157763.57	158180.60	159317.96	161151.02

Continued on next page

Continued from previous page

Parameter	Unit	0.5/0.5	0.4/0.6	0.3/0.7	0.2/0.8	0.1/0.9
Initial investment	€	48401.96	48803.09	49412.41	50459.19	52226.07
Payback time	years	N/A	N/A	N/A	N/A	N/A
Cumulative operating loss	€	64004.67	63847.07	63489.69	63658.04	63781.06
Total loss (CAPEX + extra OPEX)	€	112406.63	112650.16	112902.10	114117.23	116007.13
Maximum H_2 produced	kg	0.6061	0.6061	0.6061	0.6061	0.6061
Total H_2 produced	kg	542.98	547.54	553.14	558.03	562.76
OPEX breakdown						
Total OPEX	€	3244.50	3247.93	3253.14	3262.09	3277.20
PV	€	96.00	96.00	96.00	96.00	96.00
rSOC	€	3107.28	3107.28	3107.28	3107.28	3107.28
H_2 tank	€	41.05	44.48	49.69	58.64	73.74
TES	€	0	0	0	0	0
Cables	€	0.17	0.17	0.17	0.17	0.17
CAPEX breakdown						
Total CAPEX	€	30016.00	30358.97	30879.93	31774.92	33285.59
rSOC	€	25894.00	25894.00	25894.00	25894.00	25894.00
H_2 tank	€	4104.68	4447.65	4968.61	5863.60	7374.27
TES	€	0	0	0	0	0
Cables	€	17.32	17.32	17.32	17.32	17.32
Replacement costs						
PV	€	850.47	850.47	850.47	850.47	850.47
rSOC	€	16837.79	16837.79	16837.79	16837.79	16837.79
H_2 tank	€	696.16	754.32	842.68	994.47	1250.68
TES	€	0	0	0	0	0
Cables	€	1.53	1.53	1.53	1.53	1.53
System sizing						
Maximum stored H_2	kg	4.13918	4.48503	5.01036	5.91287	7.43624

Continued on next page

Continued from previous page

Parameter	Unit	0.5/0.5	0.4/0.6	0.3/0.7	0.2/0.8	0.1/0.9
Installed H_2 tank capacity	kg	4.13918	4.48503	5.01036	5.91287	7.43624
Economic performance comparison						
Reference annual energy cost	€			4622.27		
Annual energy cost with the proposed system	€	6755.76	6750.51	6738.60	6744.21	6748.31
Additional annual cost	€	2133.49	2128.24	2116.33	2121.94	2126.04
Relative cost increase	%	46.16	46.04	45.79	45.91	46.00
CO_2 emissions without the system						
Electricity from the grid	kg CO_2/year			9057.08		
Gas consumption	kg CO_2/year			7912.72		
Total emissions	kg CO_2/year			16969.80		
CO_2 emissions with the system						
Electricity from the grid	kg CO_2/year	5843.60	5816.59	5783.47	5754.52	5726.50
Gas consumption	kg CO_2/year	7903.19	7903.11	7903.01	7902.92	7902.84
Total emissions	kg CO_2/year	13746.79	13719.70	13686.48	13657.44	13629.34
Emission reduction	kg CO_2/year	3223.01	3250.10	3283.32	3312.36	3340.46
Emission reduction	%	18.99	19.15	19.35	19.52	19.68
Electricity purchased from the grid						
Total electricity purchased	kWh	24552.92	24439.45	24300.31	24178.66	24060.91

Continued on next page

Continued from previous page

Parameter	Unit	0.5/0.5	0.4/0.6	0.3/0.7	0.2/0.8	0.1/0.9
Cost of electricity purchased	€	1803.57	1794.78	1778.42	1775.68	1763.89
Maximum electricity purchased in one time step	kWh	8.99797	9.06914	9.06914	9.06914	9.12792
Average electricity purchased per time step	kWh	2.79519	2.78227	2.76643	2.75258	2.73917
Time step of maximum grid purchase	–	7538	6409	6156	6306	6262
Thermal balance						
Heat produced by boilers	kWh	43424.10	43423.66	43423.12	43422.65	43422.19
Cost of gas purchased	€	1707.69	1707.80	1707.04	1706.44	1707.22
Heat produced by rSOC (SOFC mode)	kWh	18610.95	18767.40	18959.19	19126.88	19289.17
Heat absorbed by rSOC (SOEC mode)	kWh	-18558.58	-18714.59	-18905.84	-19073.06	-19234.90
Heat produced by TES (discharge)	kWh	0	0	0	0	0
Heat absorbed by TES (charge)	kWh	0	0	0	0	0
TES charging energy, Q_{in}	kWh	0	0	0	0	0
TES discharging energy, Q_{out}	kWh	0	0	0	0	0
Variation in TES stored energy	kWh	0	0	0	0	0

Continued on next page

Continued from previous page

Parameter	Unit	0.5/0.5	0.4/0.6	0.3/0.7	0.2/0.8	0.1/0.9
Maximum boiler power	kW			31.45		
Time step of maximum gas purchase	–	5861	5029	4939	5040	2967

Table B.4: Main results for the 12 kWp, emission reduction maximization.

Parameter	Unit	Value
General results		
Net present cost (NPC)	€	303786.38
Initial investment	€	180080.12
Payback time	years	N/A
Cumulative operating loss	€	91253.78
Total loss (CAPEX + extra OPEX)	€	271333.90
Heat produced by boilers	kWh_{th}	43411.21
Maximum H_2 produced	kg	0.6061
Total H_2 produced	kg	676.5872
OPEX breakdown		
Total OPEX	€	4370.37
PV	€	96.00
rSOC	€	3107.28
H_2 tank	€	1166.48
TES	€	0
Cables	€	0.61
CAPEX breakdown		
Total CAPEX	€	1192602.93
rSOC	€	25894.00
H_2 tank	€	1166647.88
TES	€	0
Cables	€	61.05

Continued on next page

Continued from previous page

Parameter	Unit	Value
Replacement costs		
PV	€	850.47
rSOC	€	16837.79
H_2 tank	€	19783.51
TES	€	0
Cables	€	5.41
System sizing		
Maximum stored H_2	kg	117.62812
Installed H_2 tank capacity	kg	117.62812
Economic performance comparison		
Reference annual energy cost	€	4622.27
Annual energy cost with the proposed system	€	7664.07
Additional annual cost	€	3041.80
Relative cost increase	%	65.81
CO_2 emissions without the system		
Electricity from the grid	kg CO_2/year	9057.08
Gas consumption	kg CO_2/year	7912.72
Total emissions	kg CO_2/year	16969.80
CO_2 emissions with the system		
Electricity from the grid	kg CO_2/year	5052.85
Gas consumption	kg CO_2/year	7900.84
Total emissions	kg CO_2/year	12953.69
Emission reduction	kg CO_2/year	4016.11
Emission reduction	%	23.67
Electricity purchased from the grid		
Total electricity purchased	kWh	21230.48
Cost of electricity purchased	€	1583.43
Maximum electricity purchased in one time step	kWh	9.17218
Average electricity purchased per time step	kWh	2.41695
Time step of maximum grid purchase	–	5919
Thermal balance		

Continued on next page

Continued from previous page

Parameter	Unit	Value
Heat produced by boilers	kWh	43411.21
Cost of gas purchased	€	1710.27
Heat produced by rSOC (SOFC mode)	kWh	23190.55
Heat absorbed by rSOC (SOEC mode)	kWh	-23125.29
Heat produced by TES (discharge)	kWh	0
Heat absorbed by TES (charge)	kWh	0
TES charging energy, Q_{in}	kWh	0
TES discharging energy, Q_{out}	kWh	0
Variation in TES stored energy	kWh	0
Maximum boiler power	kW	31.45
Time step of maximum gas purchase	–	4616

Table B.5: Values common for 18 kWp installation

Parameter	Unit	Value
Max PV forecast	kW	15.53
Total PV overproduction	kWh	30209.03
Timestep with surplus PV production	–	2111

Table B.6: Main results for the 18 kWp, total cost minimization.

Parameter	Unit	Value
General		
Net Present Cost (NPC)	€	152342.77
Initial investment	€	47929.76
Payback time	years	N/A
Cumulative operating loss	€	58527.51
Total loss	€	106457.27
Maximum H_2 produced	kg	0.6061
Total H_2 produced	kg	626.0702

Continued on next page

Continued from previous page

Parameter	Unit	Value
OPEX breakdown		
OPEX	€	3284.83
PV	€	144
rSOC	€	3107.28
Tank H_2	€	33.37
TES	€	0
Cables	€	0.17
CAPEX breakdown		
CAPEX	€	29248.70
rSOC	€	25894
Tank H_2	€	3337.38
TES	€	0
Cables	€	17.32
Replacement		
PV	€	1275.71
rSOC	€	16837.79
Tank H_2	€	566.02
TES	€	0
Cables	€	1.53
Sizing		
Maximum H_2 stored	kg	3.36543
H_2 tank capacity installed	kg	3.36543
Economic performance comparison		
Reference annual energy cost	€	4517.86
Annual cost with the proposed system	€	6468.78
Annual cost difference	€	-1950.92
Relative cost increase	%	43.18
CO_2 emissions without the system		
Electricity from the grid	kg CO_2/year	8415.46
Gas consumed	kg CO_2/year	7912.72
Total	kg CO_2/year	16328.18

Continued on next page

Continued from previous page

Parameter	Unit	Value
CO_2 emissions with the system		
Electricity from the grid	kg CO_2/year	4710.21
Gas consumed	kg CO_2/year	7901.73
Total	kg CO_2/year	12611.94
Emission reduction	kg CO_2/year	3716.24
Emission reduction	%	22.76
Electricity purchased from grid		
Total electricity purchased	kWh	19790.78
Cost of electricity purchased	€	1477.97
Average electricity purchased per time step	kWh	2.25305
Time step with grid purchase	–	5222
Thermal balance		
Heat produced by boilers	kWh	43416.08
Cost of gas	€	1705.98
Heat produced by rSOC (SOFC)	kWh	21459.02
Heat absorbed by rSOC (SOEC)	kWh	-21398.64
Heat produced by TES (discharge)	kWh	0
Heat absorbed by TES (charge)	kWh	0
TES charging energy, Q_{in}	kWh	0
TES discharging energy, Q_{out}	kWh	0
Variation in TES stored energy	kWh	0
Maximum power boilers	kW	31.45
Time step with gas purchase	–	4879

Table B.7: Main results for the 18 kWp case, under different objective-weight configurations.

Parameter	Unit	0.5/0.5	0.4/0.6	0.3/0.7	0.2/0.8	0.1/0.9
General results						
Net present cost (NPC)	€	153176.20	153959.12	154384.56	157088.70	162359.31

Continued on next page

Continued from previous page

Parameter	Unit	0.5/0.5	0.4/0.6	0.3/0.7	0.2/0.8	0.1/0.9
Initial investment	€	49243.28	50151.79	50602.07	53392.22	58425.52
Payback time	years	N/A	N/A	N/A	N/A	N/A
Cumulative operating loss	€	57632.70	57399.29	57353.12	57193.27	57634.35
Total loss (CAPEX + extra OPEX)	€	106875.98	107551.08	107955.19	110585.49	116059.86
Maximum H_2 produced	kg			0.6061		
Total H_2 produced	kg	673.88	684.87	688.56	701.61	718.63
OPEX breakdown						
Total OPEX	€	3296.06	3303.83	3307.68	3331.53	3374.57
PV	€	144	144	144	144	144
rSOC	€	3107.28	3107.28	3107.28	3107.28	3107.28
H_2 tank	€	44.60	52.37	56.22	80.08	123.11
TES	€	0	0	0	0	0
Cables	€	0.17	0.17	0.17	0.17	0.17
CAPEX breakdown						
Total CAPEX	€	30371.76	31148.52	31533.51	33919.07	38222.50
rSOC	€	25894	25894	25894	25894	25894
H_2 tank	€	4460.44	5237.20	5622.19	8007.75	12311.18
TES	€	0	0	0	0	0
Cables	€	17.32	17.32	17.32	17.32	17.32
Replacement costs						
PV	€	1275.71	1275.71	1275.71	1275.71	1275.71
rSOC	€	16837.79	16837.79	16837.79	16837.79	16837.79
H_2 tank	€	756.49	888.23	953.52	1358.12	2087.98
TES	€	0	0	0	0	0
Cables	€	1.53	1.53	1.53	1.53	1.53
System sizing						
Maximum stored H_2	kg	4.49792	5.28121	5.66943	8.07504	12.41464

Continued on next page

Continued from previous page

Parameter	Unit	0.5/0.5	0.4/0.6	0.3/0.7	0.2/0.8	0.1/0.9
Installed H_2 tank capacity	kg	4.49792	5.28121	5.66943	8.07504	12.41464
Economic performance comparison						
Reference annual energy cost	€			4517.94		
Annual energy cost with the proposed system	€	6439.03	6431.25	6429.71	6424.39	6439.09
Additional annual cost	€	1921.09	1913.31	1911.77	1906.45	1921.15
Relative cost increase	%	42.52	42.35	42.32	42.20	42.52
CO_2 emissions without the system						
Electricity from the grid	kg CO_2/year			8415.63		
Cost of electricity purchased	€	1437.04	1421.85	1416.50	1388.25	1359.35
Gas consumption	kg CO_2/year			7912.72		
Total emissions	kg CO_2/year			16328.35		
CO_2 emissions with the system						
Electricity from the grid	kg CO_2/year	4427.45	4362.36	4340.56	4263.29	4162.56
Gas consumption	kg CO_2/year	7900.34	7900.70	7900.63	7900.40	7900.10
Total emissions	kg CO_2/year	12327.79	12263.06	12241.19	12163.69	12062.66
Emission reduction	kg CO_2/year	4000.56	4065.29	4087.16	4164.66	4265.69
Emission reduction	%	24.50	24.90	25.03	25.51	26.12
Electricity purchased from the grid						

Continued on next page

Continued from previous page

Parameter	Unit	0.5/0.5	0.4/0.6	0.3/0.7	0.2/0.8	0.1/0.9
Total electricity purchased	kWh	18602.72	18329.25	18237.64	17912.97	17489.76
Maximum electricity purchased in one time step	kWh	8.99681	8.99681	8.54943	8.37833	8.21619
Average electricity purchased per time step	kWh	2.1178	2.08666	2.07623	2.03927	1.99109
Time step of maximum grid purchase	–	5011	4969	4964	4945	4900
Thermal balance						
Heat produced by boilers	kWh	43411.47	43410.41	43410.06	43408.80	43407.16
Cost of gas purchased	€	1705.94	1705.58	1705.54	1704.61	1705.18
Heat produced by rSOC (SOFC mode)	kWh	23097.66	23474.61	23534.47	24048.40	24631.75
Heat absorbed by rSOC (SOEC mode)	kWh	-23032.66	-23408.56	-23534.47	-23980.73	-24562.43
Heat produced by TES (discharge)	kWh	0	0	0	0	0
Heat absorbed by TES (charge)	kWh	0	0	0	0	0
TES charging energy, Q_{in}	kWh	0	0	0	0	0
TES discharging energy, Q_{out}	kWh	0	0	0	0	0
Variation in TES stored energy	kWh	0	0	0	0	0

Continued on next page

Continued from previous page

Parameter	Unit	0.5/0.5	0.4/0.6	0.3/0.7	0.2/0.8	0.1/0.9
Maximum boiler power	kW			31.45		
Time step of maximum gas purchase	–	4735	4704	4682	4608	4532

Table B.8: Main results for the 18 kWp, emission reduction maximization.

Parameter	Unit	Value
General results		
Net present cost (NPC)	€	299243.74
Initial investment	€	178921.14
Payback time	years	N/A
Cumulative operating loss	€	88094.78
Total loss (CAPEX + extra OPEX)	€	267015.92
Maximum H_2 produced	kg	0.6061
Total H_2 produced	kg	752.714
OPEX breakdown		
Total OPEX	€	4404.80
PV	€	144
rSOC	€	3107.28
H_2 tank	€	1153.26
TES	€	0
Cables	€	0.26
CAPEX breakdown		
Total CAPEX	€	141246.02
rSOC	€	25894
H_2 tank	€	115326.01
TES	€	0
Cables	€	26.01
Replacement costs		

Continued on next page

Continued from previous page

Parameter	Unit	Value
PV	€	1275.71
rSOC	€	16837.79
H_2 tank	€	19559.32
TES	€	0
Cables	€	2.30
System sizing		
Maximum stored H_2	kg	116.29514
Installed H_2 tank capacity	kg	116.29514
Economic performance comparison		
Reference annual energy cost	€	4517.94
Annual energy cost with the proposed system	€	7454.44
Additional annual cost	€	2936.50
Relative cost increase	%	65.00
CO_2 emissions without the system		
Electricity from the grid	kg CO_2/year	8415.63
Gas consumption	kg CO_2/year	7912.72
Total emissions	kg CO_2/year	16328.35
CO_2 emissions with the system		
Electricity from the grid	kg CO_2/year	3960.87
Gas consumption	kg CO_2/year	7899.50
Total emissions	kg CO_2/year	11860.37
Emission reduction	kg CO_2/year	4467.98
Emission reduction	%	27.36
Electricity purchased from the grid		
Total electricity purchased	kWh	16642.30
Cost of electricity purchased	€	1342.60
Average electricity purchased per time step	kWh	1.89462
Time step of maximum grid purchase	–	4757
Thermal balance		
Heat produced by boilers	kWh	43403.87
Cost of gas purchased	€	1707.03

Continued on next page

Continued from previous page

Parameter	Unit	Value
Heat produced by rSOC (SOFC mode)	kWh	25799.87
Heat absorbed by rSOC (SOEC mode)	kWh	-25727.27
Heat produced by TES (discharge)	kWh	0
Heat absorbed by TES (charge)	kWh	0
TES charging energy, Q_{in}	kWh	0
TES discharging energy, Q_{out}	kWh	0
Variation in TES stored energy	kWh	0
Maximum boiler power	kW	31.45
Time step of maximum gas purchase	–	4427

Table B.9: Values common for 24 kWp installation

Parameter	Unit	Value
Max PV forecast	kW	20.7
Total PV overproduction	kWh	49239.85
Timestep with surplus PV production	–	2462

Table B.10: Main results for the 24 kWp, total cost minimization.

Parameter	Unit	Value
General		
Net Present Cost (NPC)	€	152233.82
Initial investment	€	48377.40
Payback time	years	N/A
Cumulative operating loss	€	58459.13
Total loss	€	106836.53
Maximum H_2 produced	kg	0.6061
Total H_2 produced	kg	634.9333
OPEX breakdown		
OPEX	€	3333.02

Continued on next page

Continued from previous page

Parameter	Unit	Value
PV	€	192
rSOC	€	3107.28
Tank H_2	€	33.57
TES	€	0
Cables	€	0.17
CAPEX breakdown		
CAPEX	€	29267.85
rSOC	€	25894
Tank H_2	€	3356.53
TES	€	0
Cables	€	17.32
Replacement		
PV	€	1700.94
rSOC	€	16837.79
Tank H_2	€	569.27
TES	€	0
Cables	€	1.53
Sizing		
Maximum H_2 stored	kg	3.38474
H_2 tank capacity installed	kg	3.38474
Economic performance comparison		
Reference annual energy cost	€	4485.66
Annual cost with the proposed system	€	6434.29
Annual cost difference	€	-1948.63
Relative cost increase	%	43.44
CO_2 emissions without the system		
Electricity from the grid	kg CO_2/year	8082.71
Gas consumed	kg CO_2/year	7912.72
Total	kg CO_2/year	15995.43
CO_2 emissions with the system		
Electricity from the grid	kg CO_2/year	4325.011

Continued on next page

Continued from previous page

Parameter	Unit	Value
Gas consumed	kg CO_2/year	7901.57
Total	kg CO_2/year	12226.581
Emission reduction	kg CO_2/year	3768.849
Emission reduction	%	23.56
Electricity purchased from grid		
Total electricity purchased	kWh	18172.3
Cost of electricity purchased	€	1395.61
Average electricity purchased per time step	kWh	2.0688
Time step with grid purchase	–	4879
Thermal balance		
Heat produced by boilers	kWh	43415.23
Cost of gas purchased	€	1705.67
Heat produced by rSOC (SOFC)	kWh	21762.84
Heat absorbed by rSOC (SOEC)	kWh	-21701.6
Heat produced by TES (discharge)	kWh	0
Heat absorbed by TES (charge)	kWh	0
TES charging energy, Q_{in}	kWh	0
TES discharging energy, Q_{out}	kWh	0
Variation in TES stored energy	kWh	0
Maximum power boilers	kW	32.3
Time step with gas purchase	–	4921

Table B.11: Main results for the 24 kWp case, under different objective-weight configurations.

Parameter	Unit	0.5/0.5	0.4/0.6	0.3/0.7	0.2/0.8	0.1/0.9
General results						
Net present cost (NPC)	€	153461.45	154177.22	156666.17	158103.54	163959.00
Initial investment	€	50304.79	51112.57	53800.50	55296.86	60878.93
Payback time	years	N/A	N/A	N/A	N/A	N/A

Continued on next page

Continued from previous page

Parameter	Unit	0.5/0.5	0.4/0.6	0.3/0.7	0.2/0.8	0.1/0.9
Cumulative operating loss	€	57158.14	56987.13	56617.30	56507.67	57015.80
Total loss (CAPEX + extra OPEX)	€	107462.94	108099.70	110417.80	111804.53	117894.73
Maximum H_2 produced	kg			0.6061		
Total H_2 produced	kg	696.42	706.20	727.40	735.33	750.52
OPEX breakdown						
Total OPEX	€	3349.50	3356.40	3379.39	3392.18	3439.91
PV	€	192	192	192	192	192
rSOC	€	3107.28	3107.28	3107.28	3107.28	3107.28
H_2 tank	€	50.04	56.95	79.93	92.73	140.45
TES	€	0	0	0	0	0
Cables	€	0.17	0.17	0.17	0.17	0.17
CAPEX breakdown						
Total CAPEX	€	30915.76	31606.41	33904.57	35183.95	39956.58
rSOC	€	25894	25894	25894	25894	25894
H_2 tank	€	5004.44	5695.09	7993.25	9272.63	14045.26
TES	€	0	0	0	0	0
Cables	€	17.32	17.32	17.32	17.32	17.32
Replacement costs						
PV	€	1700.94	1700.94	1700.94	1700.94	1700.94
rSOC	€	16837.79	16837.79	16837.79	16837.79	16837.79
H_2 tank	€	848.76	965.89	1355.66	1572.64	2382.08
TES	€	0	0	0	0	0
Cables	€	1.53	1.53	1.53	1.53	1.53
System sizing						
Maximum stored H_2	kg	5.0465	5.74295	8.06042	9.35055	14.16328
Installed H_2 tank capacity	kg	5.0465	5.74295	8.06042	9.35055	14.16328
Economic performance comparison						

Continued on next page

Continued from previous page

Parameter	**Unit**	**0.5/0.5**	**0.4/0.6**	**0.3/0.7**	**0.2/0.8**	**0.1/0.9**
Reference annual energy cost	€			4485.67		
Annual energy cost with the proposed system	€	6390.94	6385.24	6372.91	6369.26	6386.20
Additional annual cost	€	1905.27	1899.57	1887.24	1883.59	1900.53
Relative cost increase	%	42.47	42.35	42.07	41.99	42.37
CO_2 emissions without the system						
Electricity from the grid	kg CO_2/year			8082.76		
Gas consumption	kg CO_2/year			7912.72		
Total emissions	kg CO_2/year			15995.48		
CO_2 emissions with the system						
Electricity from the grid	kg CO_2/year	3961.16	3903.30	3777.84	3730.86	3640.97
Gas consumption	kg CO_2/year	7900.49	7900.32	7899.95	7899.81	7899.54
Total emissions	kg CO_2/year	11861.65	11803.62	11677.79	11630.67	11540.51
Emission reduction	kg CO_2/year	4133.83	4191.86	4317.69	4364.81	4454.97
Emission reduction	%	25.84	26.21	26.99	27.29	27.85
Electricity purchased from the grid						
Total electricity purchased	kWh	16643.53	16400.42	15873.28	15675.87	15298.20
Cost of electricity purchased	€	1336.36	1324.05	1289.92	1273.74	1243.04

Continued on next page

Continued from previous page

Parameter	Unit	0.5/0.5	0.4/0.6	0.3/0.7	0.2/0.8	0.1/0.9
Maximum electricity purchased in one time step	kWh	8.37833	8.37833	8.37833	8.3346	8.01366
Average electricity purchased per time step	kWh	1.89476	1.86708	1.80707	1.78459	1.7416
Time step of maximum grid purchase	–	4623	4585	4514	4491	4450
Thermal balance						
Heat produced by boilers	kWh	43409.30	43408.36	43406.31	43405.55	43404.08
Cost of gas purchased	€	1705.08	1704.79	1703.61	1703.18	1703.25
Heat produced by rSOC (SOFC mode)	kWh	23870.38	24205.47	24932.08	25204.18	25724.76
Heat absorbed by rSOC (SOEC mode)	kWh	-23803.21	-24137.36	-24861.92	-25133.26	-25652.37
Heat produced by TES (discharge)	kWh	0	0	0	0	0
Heat absorbed by TES (charge)	kWh	0	0	0	0	0
TES charging energy, Q_{in}	kWh	0	0	0	0	0
TES discharging energy, Q_{out}	kWh	0	0	0	0	0
Variation in TES stored energy	kWh	0	0	0	0	0
Maximum boiler power	kW			34.57		

Continued on next page

Continued from previous page

Parameter	Unit	0.5/0.5	0.4/0.6	0.3/0.7	0.2/0.8	0.1/0.9
Time step of maximum gas purchase	–	4764	4738	4669	4637	4569

Table B.12: Main results for the 24 kWp, emission reduction maximization.

Parameter	Unit	Value
General results		
Net present cost (NPC)	€	289450.45
Initial investment	€	170805.81
Payback time	years	N/A
Cumulative operating loss	€	85944.29
Total loss (CAPEX + extra OPEX)	€	256750.10
Maximum H_2 produced	kg	0.6061
Total H_2 produced	kg	761.5859
OPEX breakdown		
Total OPEX	€	4379.80
PV	€	192
rSOC	€	3107.28
H_2 tank	€	1079.99
TES	€	0
Cables	€	0.52
CAPEX breakdown		
Total CAPEX	€	133945.72
rSOC	€	25894
H_2 tank	€	107999.31
TES	€	0
Cables	€	52.41
Replacement costs		
PV	€	1700.94
rSOC	€	16837.79

Continued on next page

Continued from previous page

Parameter	Unit	Value
H_2 tank	€	18316.71
TES	€	0
Cables	€	4.64
System sizing		
Maximum stored H_2	kg	108.90689
Installed H_2 tank capacity	kg	108.90689
Economic performance comparison		
Reference annual energy cost	€	4485.67
Annual energy cost with the proposed system	€	7350.48
Additional annual cost	€	2864.81
Relative cost increase	%	63.87
CO_2 emissions without the system		
Electricity from the grid	kg CO_2/year	8082.77
Gas consumption	kg CO_2/year	7912.72
Total emissions	kg CO_2/year	15995.49
CO_2 emissions with the system		
Electricity from the grid	kg CO_2/year	3575.50
Gas consumption	kg CO_2/year	7899.35
Total emissions	kg CO_2/year	11474.85
Emission reduction	kg CO_2/year	4520.64
Emission reduction	%	28.26
Electricity purchased from the grid		
Total electricity purchased	kWh	15023.1
Cost of electricity purchased	€	1262.50
Maximum electricity purchased in one time step	kWh	9.12792
Average electricity purchased per time step	kWh	1.71028
Time step of maximum grid purchase	–	4388
Thermal balance		
Heat produced by boilers	kWh	43403.01
Cost of gas purchased	€	1708.19
Heat produced by rSOC (SOFC mode)	kWh	26103.96

Continued on next page

Continued from previous page

Parameter	**Unit**	**Value**
Heat absorbed by rSOC (SOEC mode)	kWh	-26030.51
Heat produced by TES (discharge)	kWh	0
Heat absorbed by TES (charge)	kWh	0
TES charging energy, Q_{in}	kWh	0
TES discharging energy, Q_{out}	kWh	0
Variation in TES stored energy	kWh	0
Maximum boiler power	kW	34.57
Time step of maximum gas purchase	–	4573